Air Force Institute of Technology

AFIT Scholar

3-2006

Doppler Aliasing Reduction in Wide-Angle Synthetic Aperture Radar Using Phase Modulated Random Stepped-Frequency Waveforms

Andrew W. Hyatt

Recommended Citation

www.manaraa.com

Doppler Aliasing Reduction In Wide-Angle
Synthetic Aperture Radar Using Phase Modulated
Random Stepped-Frequency Waveforms

THESIS

Andrew W. Hyatt, Captain, USAF

AFIT/GE/ENG/06-23

DEPARTMENT OF THE AIR FORCE
AIR UNIVERSITY

AIR FORCE INSTITUTE OF TECHNOLOGY

Wright-Patterson Air Force Base, Ohio

APPROVED FOR PUBLIC RELEASE; DISTRIBUTION UNLIMITED.

The views expressed in this thesis are those of the author and do not reflect the official policy or position of the United States Air Force, Department of Defense, or the United States Government.

AFIT/GE/ENG/06-23

Doppler Aliasing Reduction In Wide-Angle
Synthetic Aperture Radar Using Phase Modulated
Random Stepped-Frequency Waveforms

THESIS

Presented to the Faculty

Department of Electrical and Computer Engineering

Graduate School of Engineering and Management

Air Force Institute of Technology

Air University

Air Education and Training Command

In Partial Fulfillment of the Requirements for the

Degree of Master of Science in Electrical Engineering

Andrew W. Hyatt, B.S.E.E.

Captain, USAF

March 2006

Doppler Aliasing Reduction In Wide-Angle Synthetic Aperture Radar Using Phase Modulated Random Stepped-Frequency Waveforms

Andrew W. Hyatt, B.S.E.E.

Captain, USAF

Approved:

/signed/	3 Mar 2006
Maj Todd B. Hale, PhD (Chairman)	Date
/signed/	3 Mar 2006
Dr. Michael A. Temple (Member)	Date
/signed/	3 Mar 2006
Dr. Michael J. Havrilla (Member)	Date

Abstract

This research investigates the benefits of using several phase modulated Random Stepped Frequency (RSF) waveforms in a Wide-Angle Synthetic Aperture Radar (WA-SAR) scenario. RSF waveforms have been demonstrated to have desirable properties which allow for cancelling of Doppler aliased scatterers in WA-SAR images. Additional aliased energy reduction is realized by improving the uniformity of the frequency coverage across the waveform's bandwidth. Phase code modulations applied to the subpulses of a RSF waveform spread the subpulse frequency content and improve WA-SAR image quality. A length 13 Barker code applied to a RSF waveform produces an image with a 91.95% reduction in the aliased energy present relative to a WA-SAR image produced using uncoded RSF. Length 25 Frank and P4 coded RSF waveforms reduce aliased energy by 96.65% and 96.72% respectively. Additionally, phase coded RSF waveforms produce images with improved noise-free dynamic range capabilities. The Barker, Frank and P4 coded waveforms improve the noise-free dynamic range by 9.4 dB, 12.6 dB, and 12.4 dB, respectively.

Acknowledgements

Table of Contents

List of Figures

List of Tables

x

List of Symbols

List of Abbreviations

Doppler Aliasing Reduction In Wide-Angle Synthetic Aperture Radar Using Phase Modulated Random Stepped-Frequency Waveforms

I. Introduction

Synthetic Aperture Radar (SAR) allows all weather day or night imaging of terrain. Imaging as much terrain as possible while simultaneously producing high resolution images is a goal of SAR operators. In the past these objectives have conflicted; SAR could either generate images of large areas with limited resolution (i.e. stripmap SAR) or obtain high resolution images with limited area coverage (i.e. spotlight SAR).

Wide-Angle SAR (WA-SAR) has been proposed to achieve both high resolution and large area coverage simultaneously. Unfortunately, operational limitations of WA-SAR introduce new challenges such as cross range aliasing. Such aliasing causes undesired degradation of WA-SAR images.

Previous research has investigated a class of waveforms known as Random Stepped Frequency (RSF) waveforms as one method of mitigating the cross range aliasing problem. [4]. RSF waveforms are effective in removing aliased energy from WA-SAR images.

Even more aliased energy reduction comes through linear frequency modulation of RSF subpulses. The further reduction results because the waveform's bandwidth is filled more uniformly [6]. Improving an uncoded RSF waveform's frequency coverage through modulation improves WA-SAR image quality.

1.1 Problem Statement

This research examines the effectiveness of applying phase coding on top of RSF waveform subpulses. Phase modulation of RSF subpulses theoretically allows more

1

uniform frequency coverage than an uncoded RSF waveform. The phase codings investigated (Barker, Frank, and P4 codes) are commonly used in digital communications for direct sequence spread spectrum systems.

The effects of changing the transmitted waveform are investigated using a computer model of a WA-SAR imaging scenario. The image scene is a set of point scatterers precisely positioned in order to show the effects of aliasing during image formation. The model produces images using different transmit waveforms. The images are then compared to determine the waveform's effect.

1.2   Assumptions

This research effort attempts to provide a realistic model. In the past, antenna pattern effects and pulse overlap on receive due to Continuous Wave (CW) operation of the radar were ignored. The model used to investigate the new waveforms eliminates these assumptions. A realistic three-dimensional antenna pattern is incorporated into the model to provide amplitude weighting to returns from different parts of the antenna beam. CW operation of WA-SAR produces overlapping pulse returns on receive. The effects of this overlap were not modeled in previous research. The model used in this research correctly overlaps the returns from consecutive pulses due to CW operation.

Range curvature effects are correctly accounted for in the model. Previous models implemented planar wavefront assumptions. Such assumptions are now entirely removed during synthetic data generation and during image formation.

Aircraft motion effects such as non-linear flight paths and varying aircraft velocity over the length of the synthetic aperture are ignored. Such variations are not significant to the research at hand as they are completely accounted for during image formation. Therefore, aircraft motion is simulated as straight and level flight at constant velocity for simplicity.

2

All targets in this research are stationary point targets. Any complex target can be represented as a series of point scatterers [5] therefore using point scatterers in the simulation is appropriate. In order to simulate the imaging of a complex target, a set of equivalent point targets can be defined and run through the model.

Electromagnetic propagation effects through the atmosphere are ignored. Atmospheric effects include refraction, absorption, noise emission and polarization rotation [5]. Atmospheric effects vary depending on platform altitude, range, frequency, elevation angle, and other factors. These effects primarily affect returned signal amplitude. The model assumes lossless propagation for simplicity.

Receiver noise is typically modeled as Additive White Gaussian Noise (AWGN). Noise is not included in this research in order to more clearly show waveform effects in WA-SAR images. Such waveform effects would be masked by inclusion of receiver noise.

A flat earth model is used in the simulation. The elevation difference over a 1 km square image is only 5 cm (using a 4/3 earth model). The terrain is assumed planar over the extent of the image being formed.

The image scene is assumed to be unchanging over the Coherent Processing Interval (CPI). The CPI is the length of time over which the radar collects data. This assumption allows coherent image formation.

Transmission and reception of pulses is modeled using the Start-Stop assumption. The aircraft remains at a single point in space during transmission and reception of a radar pulse. The aircraft position then instantaneously moves to another point in space (determined by the aircraft's stated velocity) for transmission and reception of the next pulse. This assumption allows angular direction to a target to remain constant over a pulse. At 200 m/s the simulated aircraft jumps only 10 cm between pulses. The azimuth angle from the aircraft to a stationary target at 75 km changes at most 7.64×10^{-5} degrees during a transmission and reception of a single pulse. With a wide angle antenna beam, the amplitude variation can be ignored because amplitude

variations are very small with such a small angular change. The path length from aircraft to target changes at most by 6.67×10^{-8} meters. The path length change results in the target range being misplaced very slightly in the image. The image resolution is on the order of meters for the scenario being considered therefore such an insignificant error is ignored.

1.3 Terminology

In this document, the term *scene* refers to the entire area visible to a wide-angle antenna. Various targets are placed throughout the scene at alias locations in order to show aliasing in WA-SAR images.

The term *image* refers to the reconstruction of a specific section of the scene. The image area is generally quite small compared to the entire scene extent.

The terms *target* and *scatterer* are used interchangeably throughout the document. Targets or scatterers represent any object present in the scene which reflects energy transmitted by the WA-SAR system.

The term *range* generally refers to slant range (the distance along a line running from the radar directly to a target). Range also describes the direction perpendicular to the aircraft's flight path. The term *cross range* describes the direction along the aircraft's flight path. Images have coordinates corresponding to range (distance away from the aircraft) and cross range (perpendicular to range).

1.4 Thesis Organization

The remainder of this document is divided into four chapters. Chapter II introduces the WA-SAR scenario and the techniques used for image formation. Waveforms used in previous research (Linear Frequency Modulation (LFM), Random Stepped Frequency (RSF) and RSF-LFM coded waveforms) are also introduced.

The current research effort seeks to improve WA-SAR image quality using phase coded RSF waveforms. Chapter III describes the Barker, Frank and P4 coded wave-

4

forms which seek reduce the Doppler aliasing present in SAR images. Several improvements to previous models are also presented. Chapter IV presents the WA-SAR images which are formed using the phase coded waveforms. A normalized energy metric quantifies image quality improvement over LFM and uncoded RSF images. Chapter V concludes the document by reviewing the research goals and results and identifying possible areas of future research.

II. Synthetic Aperture Radar

Synthetic Aperture Radar (SAR) forms radar images of terrain and other targets. SAR images differ from photographic images because SAR images represent reflections of transmitted electromagnetic energy rather than reflected visible or infrared light. SAR images may be formed day or night in all weather conditions. Such advantages have made SAR an important tool for anyone interested in remote sensing.

Wide-Angle SAR (WA-SAR) differs from standard SAR systems because the antenna pattern used to transmit and receive radar signals is much wider for WA-SAR. In WA-SAR the azimuthal beam width is greater than required for equal resolution in range and azimuth [7]. Typical SAR systems use antennas with less than 5 degrees of azimuthal beamwidth. WA-SAR systems can have azimuthal beamwidths up to 90 degrees or more. The basic concepts of data collection and image formation are the same for both SAR and WA-SAR.

This chapter explores the fundamental concepts involved in SAR operation and explains the Convolution/Back-Projection (CBP) method of SAR image formation. First, the scenario geometry is defined in terms of a mathematical coordinate system. Focus then turns to radar operation and the signal processing methods allowing image formation with SAR data. An explanation of the cross range aliasing problem inherent in WA-SAR follows.

The discussion then turns to how WA-SAR image quality depends on the transmit waveform. Showing WA-SAR images illustrates how the waveform properties affect the resulting images. Linear Frequency Modulation (LFM) is the most common SAR waveform in use. Unfortunately, LFM waveforms allow cross range aliasing in WA-SAR images. Random Stepped Frequency (RSF) waveforms mitigate most Doppler aliasing. RSF waveforms variants bring some additional improvement in aliased energy mitigation. Finally, a normalized energy metric quantifies actual image improvement.

2.1 SAR Geometry

SAR systems are normally placed on air- or space-born platforms because image formation relies on the relative movement between the radar and the scene. Two primary SAR modes of operation exist: strip map and spotlight. Strip map mode utilizes a fixed on-board sidelooking antenna. The antenna is generally oriented perpendicular to the platform's motion but can be pointed slightly forward or back from perpendicular (known as squint mode collection). However the on-board antenna is oriented, it does not move during radar operation. Therefore, as the platform moves, the antenna pattern illuminates a strip of the scene parallel to the platform motion. Spotlight mode operation utilizes either an on-board steerable antenna or platform motion such that the antenna pattern constantly illuminates the same portion of the scene.

Throughout the following development, a standard three-dimensional cartesian coordinate system describes the geometry of the radar. An aircraft flies in the positive x direction at a constant height in the x-z plane. The on-board antenna points in the positive y direction towards the image scene. The image scene lies in the x-y plane.

Elevation and Azimuth angles (θ and ϕ respectively) are defined from a line parallel to the y-axis intersecting the radar antenna. Azimuth angles are positive towards the positive x-axis. Positive elevation angles are towards the positive z-axis.

The rest of this document will reference the coordinate system introduced here. Elevation and azimuth angles especially play an important role in WA-SAR image formation. The next step is to introduce basic radar operation.

2.2 SAR Operation

This research attempts to utilize various waveforms to improve WA-SAR image quality. Whichever waveform is used, it is transmitted and reflections are received and processed by the radar before image formation occurs. This section will explore these aspects of SAR operation.

2.2.1   Transmit.   As the aircraft flies along its trajectory, radar pulses are transmitted periodically. The rate at which the pulses are transmitted is known as the Pulse Repetition Frequency (PRF). The location of the aircraft when a pulse is transmitted is known as a synthetic aperture location. The aircraft location is assumed stationary during transmission and reception of a pulse and then instantaneously "jumps" to the next synthetic aperture location (commonly known as the "start-stop" assumption). The start-stop assumption is appropriate when the distance to the scene being imaged is much greater than the spacing between successive aperture locations. The PRF and aircraft velocity determine the spacing of synthetic aperture locations.

The transmitted signal $s(t)$ represents a waveform with time values in the range $0 \leq t \leq \tau$. The variable τ represents the transmitted pulse length. The precise transmitted waveform is left ambiguous at this point so that any waveform may be used.

2.2.2   Receive.   The transmit waveform travels outwards to the scene being imaged and a portion of the transmitted energy is scattered back towards the radar by each scatterer in the scene. In this research, stationary point scatterers are used to represent targets. Any complex target (terrain, vehicles, buildings, etc.) can be represented as a series of point scatterers [5]. Therefore using point scatterers in the simulation is appropriate. In order to simulate the imaging of a complex target, a set of equivalent point targets can be defined and run through the model.

A Doppler frequency shift is induced on each scatterer's return due to the relative motion between the aircraft and scatterer. The Doppler frequency shift of the nth scatterer $f_{d,n}$ is defined as [9]

$$f_{d,n} = \frac{2v_{r,n}}{\lambda} = \frac{2v_a \cos \theta_n \sin \phi_n}{\lambda}, \qquad (2.1)$$

8

where $v_{r,n}$ is the relative velocity between the aircraft and the scatterer, λ is the wavelength, v_a is the aircraft's velocity (along the x-axis), and θ_n and ϕ_n represent the elevation and azimuth angles respectively to the nth target.

Returns from each scatterer arrive with a delay equal to the round-trip time to each scatterer. The received signal from the nth point scatterer $x_n(t)$ is a delayed and Doppler frequency shifted copy of the transmitted signal

$$x_n(t) = \begin{cases} A_n s\left(t - \frac{2R_n}{c}\right) e^{\left[j2\pi f_{d,n}\left(t - \frac{2R_n}{c}\right)\right]} & \frac{2R_n}{c} \le t \le \frac{2R_n}{c} + \tau, \\ 0 & \text{else,} \end{cases} \tag{2.2}$$

where A_n is the amplitude of the return from the nth scatterer, R_n is the range to the nth scatterer, and c is the speed of light in free space. Complex envelope notation is used at this point for simplicity. (Actual hardware implementation typically uses in-phase and quadrature channels on receive which can easily be represented in complex notation.) Also, note that describing $x_n(t)$ based on actual range to the target eliminates any need for a planar wavefront assumption.

The Doppler frequency shifted return from each scatterer is received and summed with other returns based on the round trip time to each scatterer. The composite return $x(t)$ from all scatterers is a summation of the individual returns from each scatterer in the scene

$$x(t) = \sum_{n=1}^{N} x_n(t). \tag{2.3}$$

2.2.3 Pulse Compression and Range Resolution. A radar's ability to resolve different targets in range (known as range resolution) depends on the transmit pulse's bandwidth. An uncompressed pulse is related to its bandwidth B by [5]

$$B \approx \frac{1}{\tau}. \tag{2.4}$$

Through modulation, a pulse of longer duration can have the same bandwidth as a pulse of shorter duration. The modulated pulse is match filtered resulting in a

compressed pulse width of $1/B$ [5]. Thus, if two pulses of different time duration occupy the same bandwidth, through matched filtering the range resolution of the two pulses can be equivalent. The process of modulating a pulse and match filtering the return is known as pulse compression. Almost all modern radars use some sort of pulse compression. The range resolution achieved when using pulse compression is expressed in terms of bandwidth as

$$\Delta R = \frac{c}{2B}. \tag{2.5}$$

In SAR imaging, it is common to design the matched filter to match the Doppler shift of a point in the center of the image being formed and accept the slight mismatch in Doppler that results. The mismatch will be small if the image size is not too large. Each pulse that is transmitted will have its own unique matched filter since the Doppler shift of the image's central point changes over the length of the aperture due to aircraft motion.

The matched filter is the complex conjugate of the time-reversed return from the image scene center. The matched filter $h(t)$ is defined as [6]

$$h(t) = \begin{cases} \left[s\left(\frac{2R_c}{c} - t\right) e^{\left[j2\pi f_{d,c}\left(\frac{2R_c}{c} - t\right)\right]} \right]^* & \frac{2R_c}{c} - \tau \leq t \leq \frac{2R_c}{c}, \\ 0 & \text{else}, \end{cases} \tag{2.6}$$

where the superscripted * represents conjugation, R_c is the range to the center of the scene being imaged, $f_{d,c}$ is the associated Doppler frequency shift of a scatterer at that location.

The matched filter output $y(t)$ is the result of convolving the received signal with the matched filter

$$y(t) = x(t) * h(t) = \int_{-\infty}^{\infty} x(w)h(t-w)dw \tag{2.7}$$

10

where $*$ represents convolution. Using Fourier transform properties Eqn. (2.7) can be expressed as

$$y(t) = \mathcal{F}^{-1}\left\{\ \mathcal{F}\{x(t)\} \times \mathcal{F}\{h(t)\}\ \right\} = \mathcal{F}^{-1}\left\{X(f)H(f)\right\} \tag{2.8}$$

where $\mathcal{F}\{\cdot\}$ is the Fourier transform operator, $\mathcal{F}^{-1}\{\cdot\}$ is the Inverse Fourier transform operator, f is frequency, and $X(f)$ and $H(f)$ are the Fourier transforms of $x(t)$ and $h(t)$ respectively. The output $y(t)$ can also be written as a function of range R using the following conversion:

$$y(R) = y\left(\frac{ct}{2}\right) \tag{2.9}$$

The function $y(R)$ is called a range profile and contains amplitude and phase data as a function of range only. A range profile is generated at each synthetic aperture location. The next processing step will be to coherently combine each of these separate returns to form an image.

2.3 Image Formation

In order to understand how an image may be formed from a set of range profiles it is helpful to reexamine the information that is available to work with. Upon transmission a radar pulse propagates outward spherically. The energy of the pulse will strike all targets that lie at equal range at the same instant, regardless of where they lie in elevation or azimuth. The same is true of the reflected signal received back at the radar. Reflections from all targets at equal ranges are received simultaneously. The radar does not distinguish between returns from different azimuth or elevation angles. Only range (or equivalently, time) information is available upon receive.

Because all points of equal range lie on a sphere centered around the radar it is easiest to transform the coordinate system from cartesian to spherical. Using a fixed coordinate system during the entire SAR collection implies that R, θ and ϕ all

11

depend on the aircraft's instantaneous location $(x_a,\ y_a,\ z_a)$ and are defined as

$$
\begin{aligned}
R &= \sqrt{(x_a - x)^2 + (y_a - y)^2 + (z_a - z)^2} \\
\theta &= \sin^{-1}\left(\frac{z_a - z}{\sqrt{(x_a - x)^2 + (y_a - y)^2 + (z_a - z)^2}}\right) \\
\phi &= \sin^{-1}\left(\frac{x_a - x}{\sqrt{(x_a - x)^2 + (y_a - y)^2}}\right)
\end{aligned}
\tag{2.10}
$$

The function $g(x,y,z)$ represents the complex reflectivity of the image scene as a function of location in the three-dimensional space. After a transformation to spherical coordinates using (2.10) the reflectivity function becomes $g(R,\theta,\phi)$. As the returns are summed or integrated over all θ and ϕ, $g(R,\theta,\phi)$ is also integrated over all θ and ϕ, or in other words, projected. The projection of $g(R,\theta,\phi)$ results in complex reflectivity values of the scene that exist on a range line extending from the aircraft to the image scene center which is described by θ_p and ϕ_p.

Using the modified spherical coordinates defined in Eqn. (2.10), the projection function at a particular collection θ_p and ϕ_p is

$$
p_{\theta_p,\phi_p}(R) = \int_\phi \int_\theta g(R,\theta,\phi)\delta(R,\theta_p,\phi_p)d\theta d\phi
\tag{2.11}
$$

where $\delta(\cdot)$ represents the Dirac delta function. Notice that $p_{\theta_p,\phi_p}(R)$ is a function of range only.

The ultimate goal of SAR imaging is to form an accurate estimate of $g(x,y,z)$. The key to obtaining this estimate is the Projection-Slice theorem. The Projection-Slice theorem relates the Fourier transform of a projection function to a trace (or line) through the Fourier transform of the original function at the same angle as the projection function. The Fourier transforms are defined as

$$
\begin{aligned}
\mathcal{F}\{g(x,y,z)\} &= G(X,Y,Z) \\
\end{aligned}
\tag{2.12}
$$

$$
\begin{aligned}
\mathcal{F}\{p_{\theta_p,\phi_p}(R)\} &= P_{\theta_p,\phi_p}(U)
\end{aligned}
\tag{2.13}
$$

12

where X, Y, Z and U represent spatial frequency variables corresponding to x, y, z and R. The Projection-Slice theorem states that $P_{\theta_p,\phi_p}(U)$ is equal to values of $G(X,Y,Z)$ on a line at the same θ and ϕ angles [2].

The usefulness of the Projection-Slice theorem becomes evident by considering a range profile again. A range profile can be expressed as the result of convolving the match filtered waveform with the one-dimensional projected reflectivity function $p_{\theta_p,\phi_p}(R)$ as

$$y(R) = [s(R) * h(R)] * p_{\theta_p,\phi_p}(R) \tag{2.14}$$

where the time-range relationship from Eqn. (2.9) has been used and Doppler frequency shifts of each scatterer are rolled into $p_{\theta_p,\phi_p}(R)$. As was done in Eqn. (2.8) the convolutions can be written as

$$\begin{aligned} \mathcal{F}^{-1}\{Y(U)\} &= \mathcal{F}^{-1}\{\mathcal{F}\{s(R)\} \times \mathcal{F}\{h(R)\} \times \mathcal{F}\{p_{\theta_p,\phi_p}(R)\}\} \\ &= \mathcal{F}^{-1}\{[S(U)H(U)]P_{\theta_p,\phi_p}(U)\}. \end{aligned} \tag{2.15}$$

The spatial frequencies contained in $S(U)$ and $H(U)$ are limited to [2]

$$\frac{4\pi}{c}f_1 \leq U \leq \frac{4\pi}{c}f_2 \tag{2.16}$$

where the values f_1 and f_2 represent the lower and upper frequencies, respectively, contained in the waveform $s(t)$. The match filtered waveform has the effect of windowing $P_{\theta_p,\phi_p}(U)$. $Y(U)$ is therefore an estimate of $P_{\theta_p,\phi_p}(U)$ based on the limited spatial frequencies which are transduced.

By the Projection-Slice theorem, Eqn. (2.15) (prior to the inverse transforms) describes samples of $\hat{G}(X,Y,Z)$, an estimate of the Fourier transform of the true scene reflectivity. As more range profiles are collected throughout the synthetic aperture, a ribbon surface of $\hat{G}(X,Y,Z)$ is obtained which is defined by the elevation and azimuth values of each profile. Obtaining $\hat{g}(x,y,z)$ is simply a matter of performing an inverse

13

Fourier transform. Generally some interpolation will be required since the Fourier transform requires uniformly spaced samples.

2.3.1 Cross Range Resolution.   Image resolution is determined from the extent of information in the spatial frequency domain. Range resolution is determined by the waveform bandwidth as discussed in Section 2.2.3. The cross range resolution ΔA is determined by the angular diversity $\Delta \phi$ over which range profiles are collected. The spatial frequency spread due to angular diversity is in the X dimension and is described as [2]

$$\Delta X = 2 \left(\frac{4\pi}{\lambda} \right) \sin(\Delta \phi / 2). \tag{2.17}$$

Since most SAR collections are taken over a small $\Delta \phi$, a small angle approximation of Eqn. (2.17) can be used. The corresponding spatial domain resolution obtained using a small angle approximation is [2]

$$\Delta A = \frac{\lambda}{2\Delta \phi}. \tag{2.18}$$

2.3.2 Convolution/Back-Projection Algorithm.   The particular method of image formation used in this research utilizes an algorithm known as Convolution/Back-Projection (CBP). CBP is a spotlight mode image formation algorithm which forms an image by focussing on a particular point in the scene (the image center). The convolution occurs in Eqn. (2.14) where the match filtered waveform is convolved with the scene's projection function.

Back-projection refers to taking $y(R)$ and projecting it's values back out into the spatial domain. The back-projection is often performed along planes which are perpendicular to $y(R)$ when the assumption of planar wavefronts is used. For this research the back-projection does not assume planar wavefronts and the values of $y(R)$ are projected out along spherical surfaces of θ and ϕ rather than planes.

The CBP algorithm forms an image using a single range profile at a time. Image pixel coordinates in this research are assumed to be located on the ground (but could

14

be in the slant plane). At each synthetic aperture location the range R_p to an image pixel with coordinates (x_p, y_p, z_p) is calculated as

$$R_p = \sqrt{(x_a - x_p)^2 + (y_a - y_p)^2 + (z_a - z_p)^2} \tag{2.19}$$

The pixel is assigned the value $y(R_p)$. Performing this assignment for every image pixel results in the complex values of $y(R)$ being back-projected along curves of equal range in the image.

At each subsequent synthetic aperture location a new image is formed using the range profile from that location. The new image is summed with the image formed at the first synthetic aperture location to produce a coherently combined image formed from the first two synthetic aperture locations. The process is repeated for every other location. The coherent addition of returns received at different angles results in increased cross-range resolution.

Now that the fundamentals of SAR operation and image formation have been reviewed the focus turns the details of WA-SAR. WA-SAR images suffer from cross range aliasing. The next section will explore why this aliasing occurs.

2.4   Wide Angle Synthetic Aperture Radar

SAR operators desire to form high resolution images of large areas of terrain. Stripmap mode operation allows the radar to see more terrain than spotlight mode (see Section 2.1). Unfortunately, traditional SAR systems with small azimuthal beamwidths can only form a synthetic aperture as long as a particular scatterer is in the antenna beam. (Longer apertures will cause the particular target to integrate out.) The length of the synthetic aperture directly affects $\Delta\phi$. Equation 2.18 shows that an increase in $\Delta\phi$ results in improved resolution. By widening the antenna beamwidth, it is possible to lengthen the synthetic aperture and increase $\Delta\phi$, resulting in higher resolution images.

WA-SAR uses stripmap mode operation combined with spotlight mode processing to form high resolution images. Each image formed covers only a small portion of the terrain scene covered by the SAR collect. Images from different parts of the scene are patched together to form high resolution images of large areas of terrain.

A side effect of increasing the azimuthal beamwidth is a large increase in the Doppler frequency shifts seen by the radar. A corresponding increase in the PRF is required in order to prevent Doppler foldover or aliasing which occurs because of under-sampling along the synthetic aperture. The PRF must be at least

$$PRF \geq (f_{d,\text{max}} - f_{d,\text{min}}) \tag{2.20}$$

in order to avoid aliasing, where $f_{d,\text{max}}$ and $f_{d,\text{min}}$ represent the maximum and minimum Doppler frequencies seen by the radar. Equation (2.20) assumes stripmap mode broadside collection with only mainbeam scatterers present [6]. Unfortunately, the range extent of the image scene imposes an upper limit on the PRF in order to avoid range aliasing [4]

$$PRF \leq \frac{c}{2\Delta R_u} \tag{2.21}$$

where ΔR_u represents the unambiguous slant range extent that is being imaged. In order to image large extents of terrain in both range and cross-range either Eqn. (2.20) or Eqn. (2.21) must be violated.

WA-SAR chooses to violate Eqn. (2.20) and sets $PRF = 1/\tau$ such that waveforms are transmitted consecutively, forming a Continuous Wave (CW) radar. In order to receive returns, a separate receive antenna is utilized.

The choice to violate Eqn. (2.20) allows Doppler aliasing to occur in WA-SAR images. The aliasing occurs at integer multiples of the PRF [4]. In order to illustrate the Doppler aliasing, a scene with nine point targets is created. Figure 2.1 shows the positioning of the targets in the scene. The point targets are positioned such that, depending on the aircraft velocity, some or all of the targets will have a normalized

Table 2.1:   Point Target Locations and Normalized Doppler Shifts

Target Number	Target Location (x_t, y_t, z_t)	Range (m)	f_d/PRF $v_a = 100$ m/s	f_d/PRF $v_a = 200$ m/s
1	(-52380, +70398, 0)	87800	-2.0	-4.0
2	(-39701, +78168, 0)	87725	-1.5	-3.0
3	(-26145, +83604, 0)	87650	-1.0	-2.0
4	(-13211, +86519, 0)	87575	-0.5	-1.0
5	(0, +87447, 0)	87500	+0.0	+0.0
6	(+13189, +86371, 0)	87425	+0.5	+1.0
7	(+26055, +83318, 0)	87350	+1.0	+2.0
8	(+39499, +77766, 0)	87275	+1.5	+3.0
9	(+52020, +69917, 0)	87200	+2.0	+4.0

Doppler frequency that is an integer multiple of the PRF. The point target coordinates (x_t, y_t, z_t) are listed in Table 2.1 as well as the normalized Doppler shift calculated at the center of the synthetic aperture. The targets have slight variations to allow scatterers to be identified in the resulting SAR images. The radar parameters used for all simulations in this research are listed in Table 2.2.

Up to this point the transmit signal has been left ambiguous. Before introducing specific waveforms, some tools for analyzing the waveforms will be introduced. Section 2.5 will introduce the most common SAR waveform–Linear Frequency Modulation (LFM). Other waveforms examined in this research effort will be compared against LFM.

2.5   Linear Frequency Modulated Waveforms

The most widely used type of pulse compression in SAR is Linear Frequency Modulation (LFM). LFM consists of a constant amplitude sinusoid defined as

$$s(t) = \Re \left\{ A_t e^{-j2\pi f_c t} e^{j\pi \frac{Bt^2}{\tau}} \right\}, \quad -\frac{\tau}{2} \leq t \leq \frac{\tau}{2} \tag{2.22}$$

where f_c is the radar's center frequency, $\Re\{\cdot\}$ indicates taking the real part and A_t is the transmit amplitude. LFM waveforms contain frequency content that uniformly

17
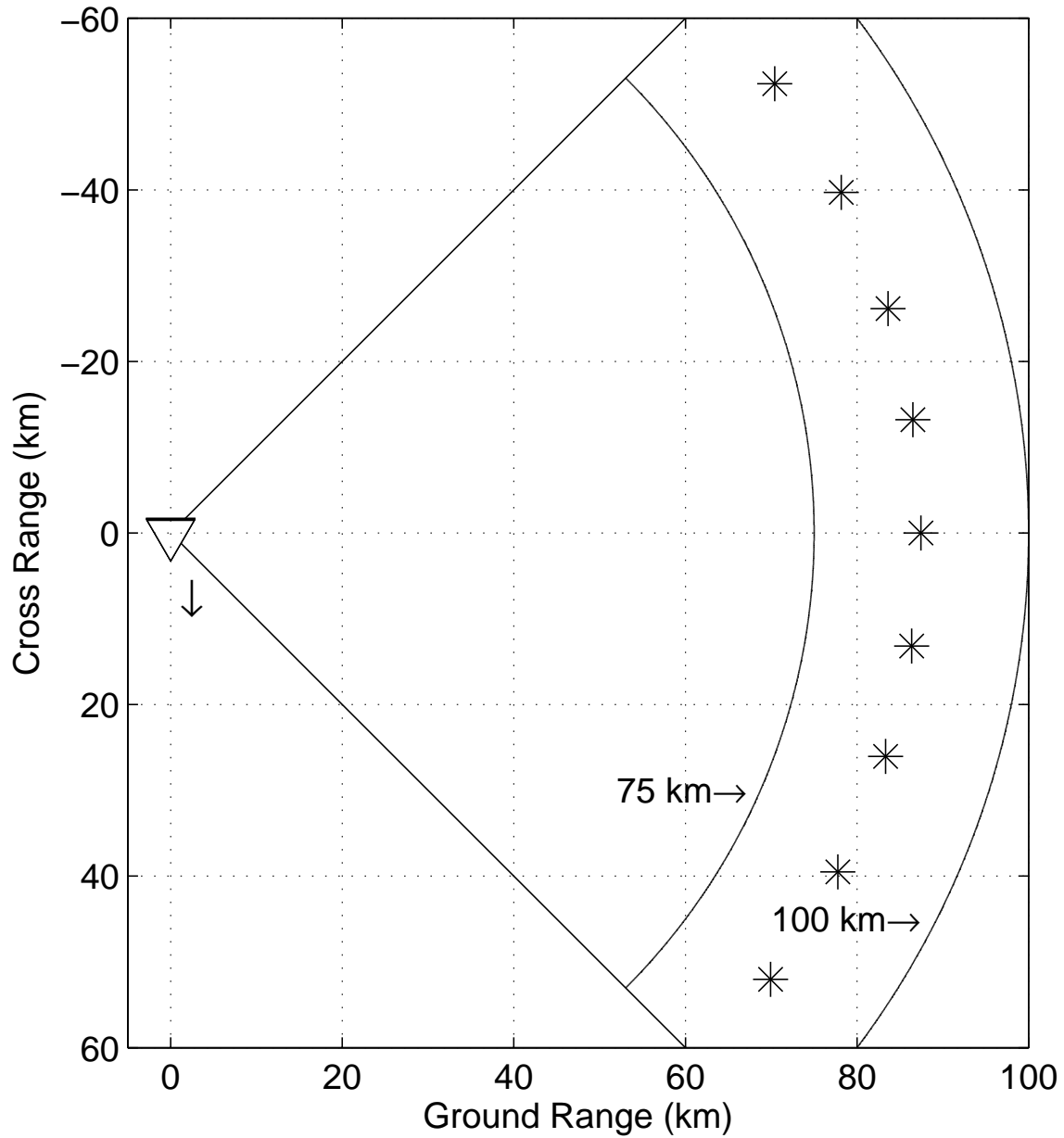
Figure 2.1: WA-SAR imaging scenario showing aircraft position, direction of motion, 90° antenna beamwidth and point scatterer locations. The range rings at 75 km and 100 km slant range indicate the range extent of the SAR collect. Exact target locations are listed in Table 2.1 and for convenience are numbered from top (target 1) to bottom (target 9) corresponding to their location in the figure. Images will be formed of a 1 km^2 area around the center target (target 5).

18

Table 2.2:   WA-SAR Simulation Parameters

Parameter	Value
Aircraft Altitude h_a	3048 m
Aircraft Velocity v_a	100 or 200 m/s
PRF	2 kHz
Synthetic Aperture Length	200 m
Antenna Element Pattern	Cosine
Antenna Azimuth Beamwidth	$90°$
Minimum Slant Range	75 km
Maximum Slant Range	100 km
Pulse Length τ	500 μsec
Number of Subpulses (for RSF waveforms)	100
Center Frequency f_c	10 GHz
Waveform Bandwidth B	20 MHz
Receiver Sampling Rate $1/t_s$	40 MHz
Speed of Light c	3×10^8 m/s
Image Extent	1 km $\times$ 1 km
Image Size (pixels)	512×512

cover the signal bandwidth. Figure 2.2 illustrates the frequency content of an LFM waveform.

2.5.1 *Ambiguity Function.*   One of the most important tools for analyzing waveforms is the ambiguity function. The ambiguity function is the squared magnitude of the matched filter output [9]

$$|\chi(T_r, f_d)|^2 = \left| \int_{-\infty}^{\infty} s(t)s^*(t + T_r)e^{-j2\pi f_d(t+T_r)}dt \right|^2 \tag{2.23}$$

where T_r represents a time delay. The ambiguity function shows how a mismatch between the received signal and the matched filter in either time or Doppler frequency affects the output of the matched filter. The ambiguity function for LFM is shown in Figure 2.3.

The LFM ambiguity diagram reveals in part why aliasing occurs. The waveform exhibits Doppler tolerance which means that the matched filter provides a strong response even if a return signal exhibits a large Doppler shift (albeit with a time

19
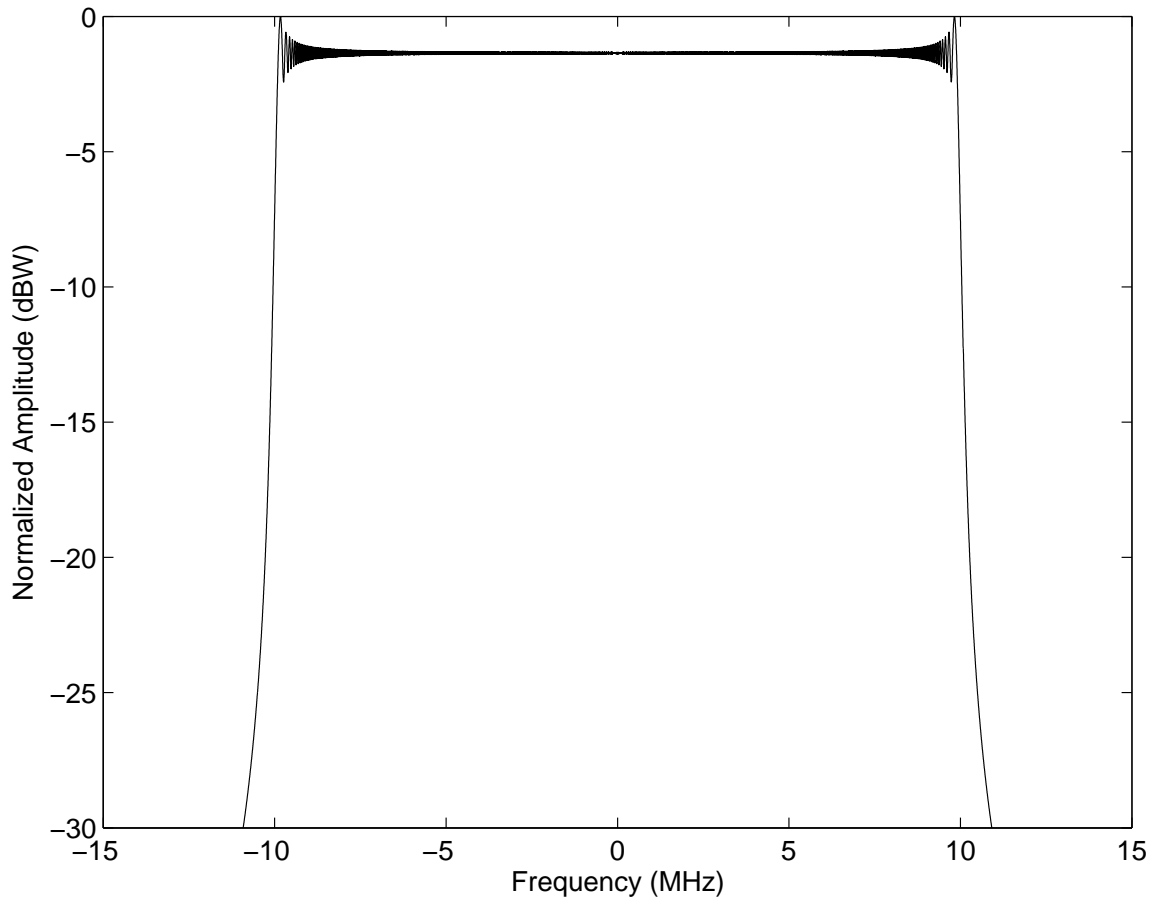
Figure 2.2: LFM frequency plot showing uniform frequency coverage. The LFM waveform has been mixed down to baseband and shows constant amplitude frequency coverage over a 20 MHz bandwidth.
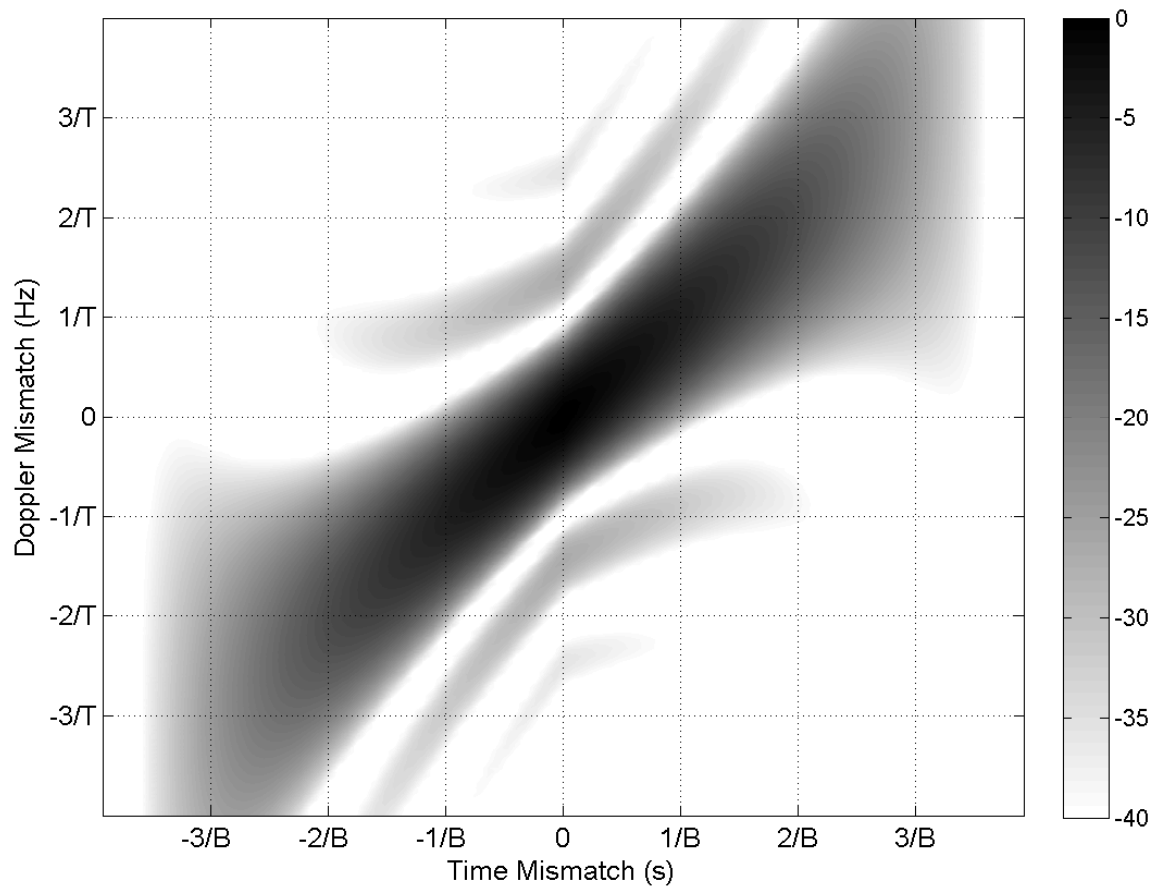
Figure 2.3: Example LFM ambiguity function plot. The length of the LFM waveform is T in this plot. The ambiguity function shows that a Doppler frequency mismatched input can still produce a significant response at the output of the matched filter. The Doppler tolerance of this waveform allows aliasing in WA-SAR images.

21

error). In WA-SAR where targets with large Doppler shifts actually lie outside of the desired image region such a response is undesireable. Due to the Doppler tolerance of LFM, the response of targets with large Doppler shifts appear in the image when they shouldn't.

2.5.2 LFM WA-SAR Images.   Figures 2.4 and 2.5 show WA-SAR images formed using a LFM waveform and the parameters in Table 2.2. In Fig. 2.4 the aircraft velocity is 100 m/s. According to Table 2.1 only the odd numbered scatterers have Doppler shifts which are integer multiples of the PRF for this aircraft velocity and it is clear that only they have aliased into the image. Figure 2.4(a) shows the two-dimensional image. Figure 2.4(b) offers an alternative view with height representing pixel amplitude. In the alternative view it is easy to see the amplitude of aliased scatterers relative to the central target.

Figure 2.5 presents the image formed when the aircraft speed in increased to 200 m/s. All nine scatterers are present in the image due to the fact that at this aircraft velocity all scatterers have Doppler shifts which are an integer multiple of the PRF.

> !   All WA-SAR images in this document are produced of a 1 km^2 region centered on scatterer 5 from Table 2.1. Only a single scatterer is physically present in the image area. The images are normalized to the peak value and floored at -60 dB (values below the -60 dB are dropped).

The point target located at the image centers is focused. Other scatterers which have aliased into the images are smeared. The smearing worsens for targets with larger Doppler shifts as the image formation process attempts to focus a scatterer which is not physically present in the image scene.

The Doppler aliasing which is present in Figures 2.4 and 2.5 seriously degrade the WA-SAR images. A class of waveforms known as Random Stepped Frequency waveforms has been shown to mitigate the aliasing problem [4,6] and will be discussed next.
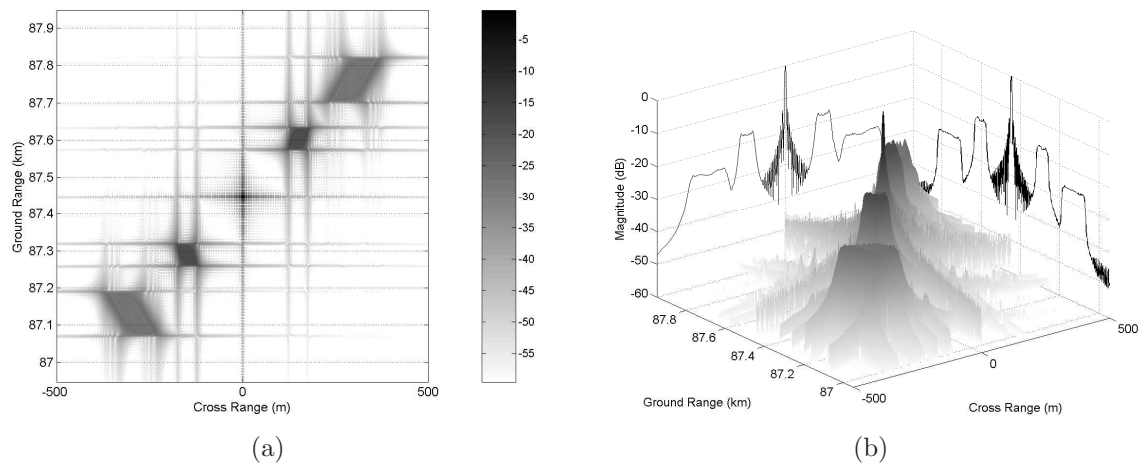
Figure 2.4: (a) SAR image generated using LFM for $v_a = 100$ m/s with 60 dB dynamic range. Only the point scatterers with Doppler shifts that are integer multiples of the PRF have aliased (See Table 2.1).
(b) Surface plot showing the relative amplitudes of the primary and aliased targets. The maximum values along ground range and cross range are projected onto the walls.
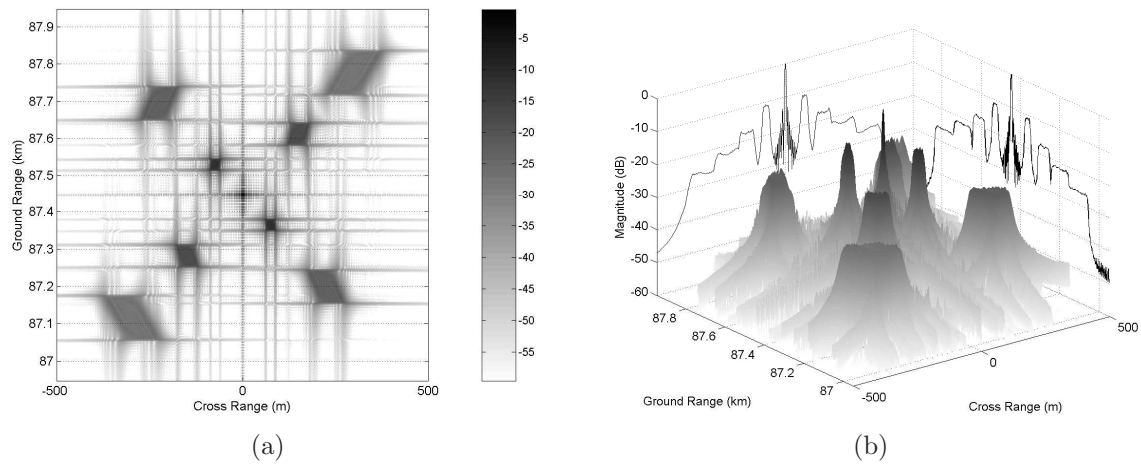

Figure 2.5: (a) SAR image generated using LFM for $v_a = 200$ m/s with 60 dB dynamic range. All scatterers have aliased into the image because they all now have Doppler shifts which are integer multiples of the PRF.
(b) Surface plot showing the relative amplitudes of the primary and aliased targets. The maximum values along ground range and cross range are projected onto the walls.

23

2.6 *Random Stepped Frequency Waveforms*

A stepped frequency waveform of duration τ is formed by combining N sub-pulses of duration $\tau_s = \tau/N$, each with a different frequency f_n. The frequencies are uniformly spaced within a bandwidth B and can be applied to the subpulses in any order. The entire transmit waveform can be written as [4]

$$s(t) = \frac{1}{\sqrt{\tau}} \sum_{n=0}^{N-1} \Pi\left(\frac{t - n\tau_s}{\tau_s}\right) \Re\left\{e^{j2\pi f_n t}\right\}, \quad -\frac{\tau}{2} \leq t \leq \frac{\tau}{2} \qquad (2.24)$$

where $\Pi(x)$ is the rectangle function defined as [1]

$$\Pi(x) = \begin{cases} 0, & |x| > \frac{1}{2} \\ 1, & |x| < \frac{1}{2} \end{cases} \qquad (2.25)$$

Random Stepped Frequency (RSF) waveforms are generated by using a random frequency on each subpulse. It is common to represent the frequency ordering using a time-frequency grid. The grid is divided into N^2 regions of size $B/N \times \tau/N$. Such a grid is shown for a single random frequency ordering in Fig. 2.6(a). The grid depicts solid covering of the time frequency space for each subpulse. In reality, only a single frequency is transmitted during each subpulse and a more accurate depiction is shown in Fig. 2.6(b).

The transmission of N distinct tones by itself would not normally be enough to adequately cover the entire bandwidth. But the limited duration of each subpulse causes the frequency coverage to be a sinc rather than a delta function [6]. The frequency content of a single subpulse is shown in Fig. 2.7. Even though a single tone is transmitted, spreading occurs due to the limited time duration of the subpulse. The frequency content of a single uncoded RSF waveform is shown in Fig. 2.8. Notice that although it is not uniform across the bandwidth like LFM, the bandwidth is covered with no visible gaps. The frequency magnitude 5 MHz outside of the waveform's bandwidth is approximately -28.7 dB.

24
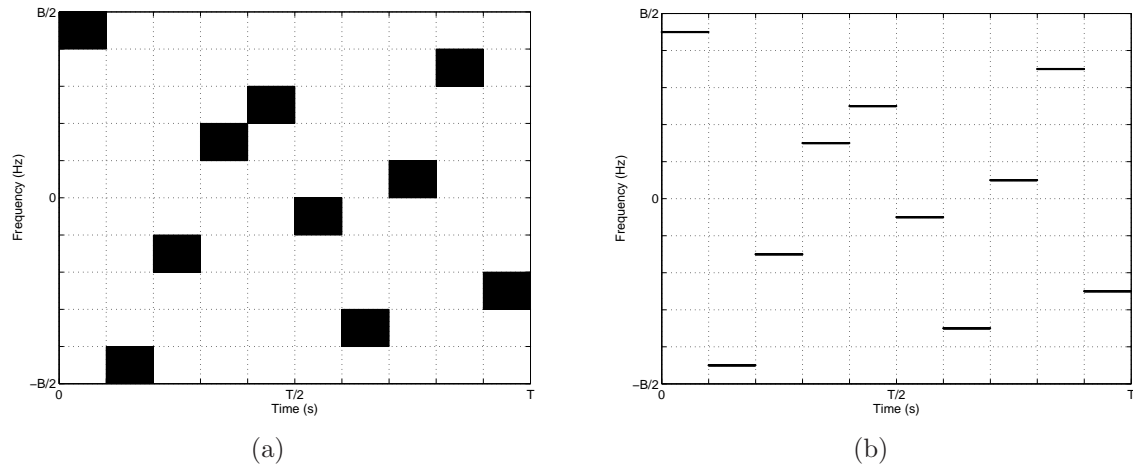
Figure 2.6: (a) RSF Time-Frequency Grid. Only 10 subpulses are used in order to illustrate the concept. The actual simulation uses 100 subpulses. Blocks indicate that frequency content in the bandwidth depicted is transmitted during a particular subpulse. For uncoded RSF, only a single tone is actually transmitted.
(b) Alternative depiction of the RSF time-frequency grid. In this figure, the actual frequency values which are transmitted during a particular subpulse are shown.
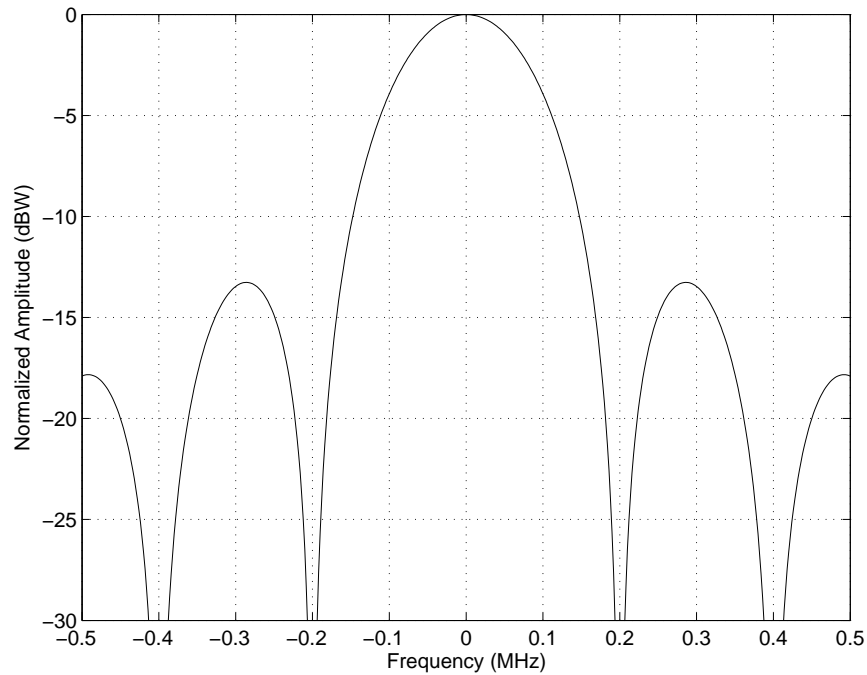
Figure 2.7: Uncoded RSF Subpulse Frequency Plot. A single frequency is transmitted during the short subpulse duration. The actual frequency content of the subpulse is attributed to the time duration of the subpulse.

25
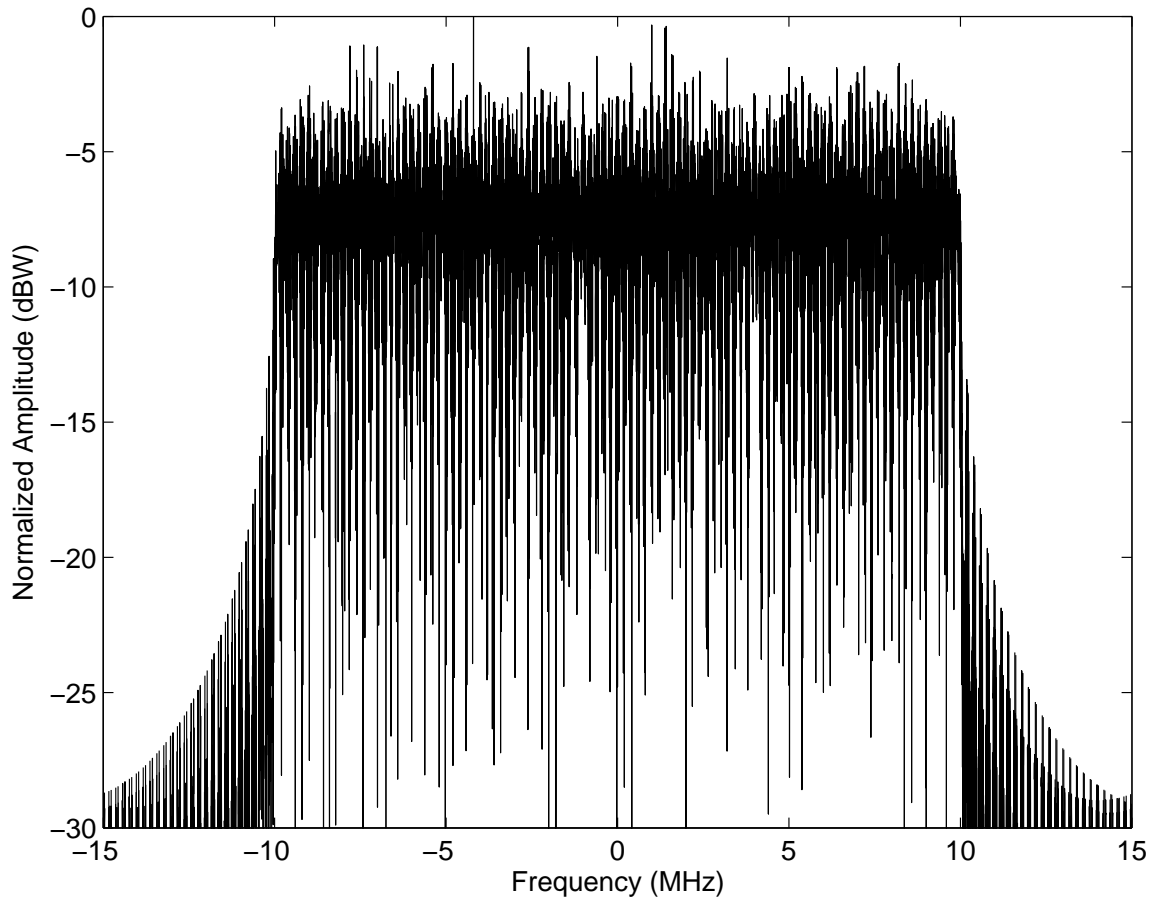
Figure 2.8: Uncoded RSF Frequency Plot. Frequency coverage across the bandwidth is much less uniform than LFM but no obvious gaps exist. Adequate coverage across the designated bandwidth is essential to Doppler aliasing reduction.

26

Given N subpulses a single RSF waveform covers only N of the N^2 possible sections of the time-frequency grid. The ambiguity function for a single RSF waveform is a thumbtack with noise-like sidelobes [9]. At each synthetic aperture location the frequency ordering is randomly chosen, eventually resulting in the complete filling of the time-frequency region when the pulses are coherently combined. As shown in [4], coherent combination of many RSF waveforms results in an ambiguity function which approaches

$$|\chi(T_r, f_d)|^2 = |\text{sinc}(BT_r)\text{sinc}(\tau f_d)|^2 \tag{2.26}$$

where $\text{sinc}(x)$ is defined as

$$\text{sinc}(x) \triangleq \frac{\sin(\pi x)}{(\pi x)} \tag{2.27}$$

Equation (2.26) is plotted in Fig. 2.9. Unlike the LFM waveform, RSF exhibits a strong response only when the received signal is closely matched by the filter (only small time or frequency shifts). When a shift in frequency exists, the amplitude of the response tapers off as $\text{sinc}(\tau f_d)$ which has nulls at $1/\tau$. Recall that the Doppler aliasing occurs at integer multiples of the PRF. It is possible to null out the alias locations by choosing PRF $= 1/\tau$ [4].

2.6.1   Uncoded RSF WA-SAR Images.   Figures 2.10 and 2.11 show two WA-SAR images formed using an uncoded RSF waveform and the parameters in Table 2.2. They show that the scatterers which would normally have aliased into the images have been effectively filtered out by the uncoded RSF waveform but a noise-like background results from each single waveform's noise-like ambiguity function. The background level in Fig. 2.10 is approximately -45.1 dB while the background level in Fig. 2.11 is approximately -41.3 dB. The noise-like pixels limit the dynamic range of the image which is the ability to see true image details.

!   Receiver noise is ignored in this research. The noise-like background present in RSF images is due entirely to waveform effects.
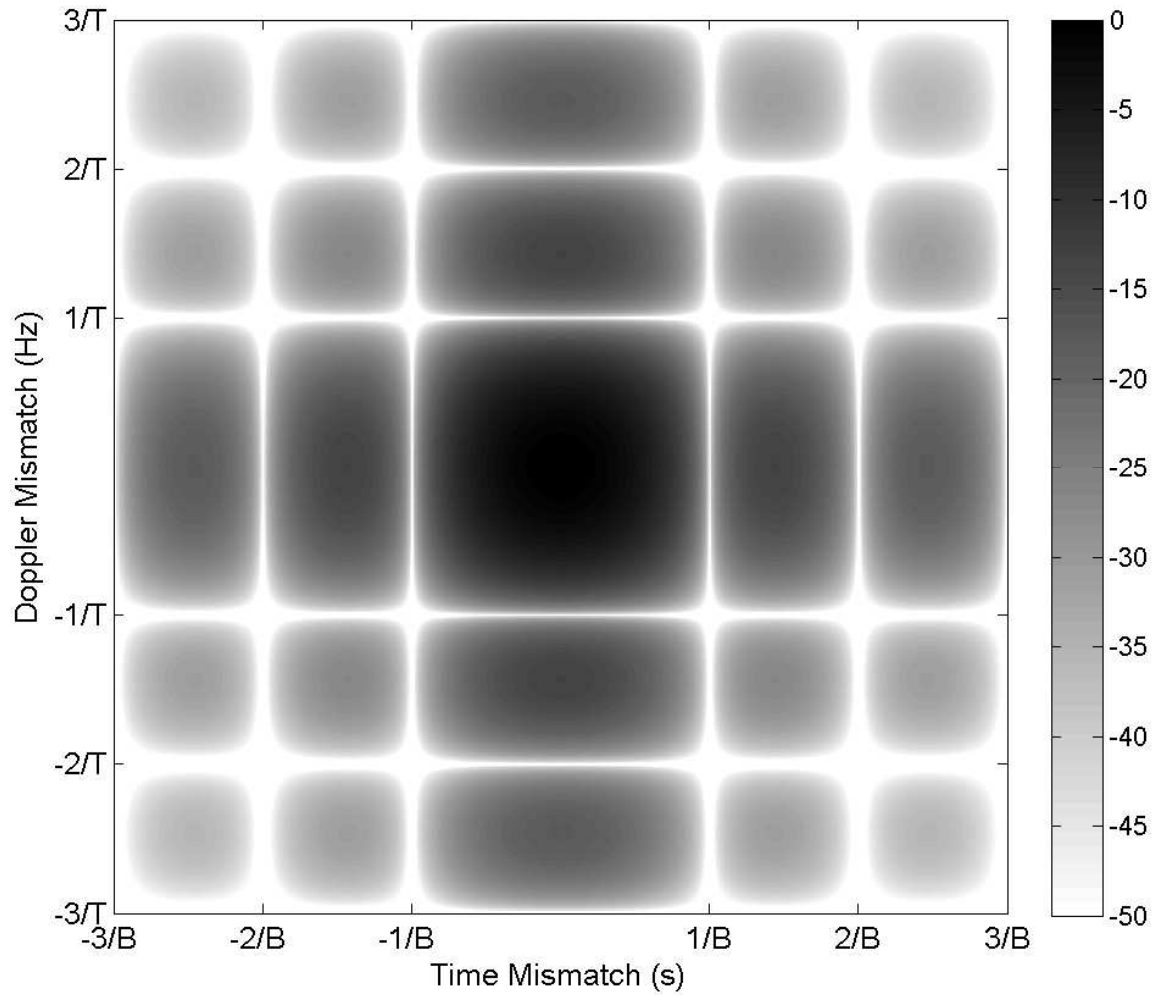
Figure 2.9: Ideal RSF ambiguity Plot. The actual ambiguity function of many RSF waveforms coherently combined *approaches* a 2-D sinc function. The nulls of this function allow cancellation scatterers located in Doppler frequency at multiples of the PRF when the PRF is chosen to be $1/\tau$.

The noise-like background present in the RSF images can be attributed primarily to the waveform's interaction with other targets in the scene. The noise-like ambiguity function of each waveform causes energy from the aliased targets to appear in the image due to relatively high sidelobe lobe levels which are present. Additionally, the aliased scatterers have Doppler Shifts which vary of the length of the synthetic aperture. The normalized Doppler shifts listed in Table 2.1 are calculated at the center of the synthetic aperture. The actual Doppler shifts vary slightly around the listed values and therefore the returns from a given scatterer may not be completely cancelled out. That the noise-like floor is due to the presence of other targets in the scene is evident form the fact that an image of a single scatterer (see Fig. 2.12) does not have the noise-like pixels present in Figs. 2.10 and 2.11. The coherent combination of many RSF waveforms effectively pushes the amplitude of the noise-like floor down but with a dynamic range of -60 dB the noise-like background seriously degrades the image.

2.6.2 Performance Metric. In order to quantify the actual improvement that the RSF waveform has, a metric needs to be established. As described in [4] and [6] a normalized energy metric can be used to quantitatively compare various waveforms. The normalization occurs with respect to the *ideal* image comprised of only the scatterer which physically resides in the image area (all other scatterers are removed during ideal image formation).

The ideal image is formed using the same waveform as is used to generate the image to be normalized. This guarantees that the scatterer of interest will be identical in both images. The single scatterer WA-SAR image used for LFM normalization is shown in Fig. 2.12. No aliasing is present in the figure because no targets exist elsewhere in the scene. The point target located at the image center is focused and exhibits a sinc structure in both range and cross-range. Figure 2.12 exhibits the image which should be produced by WA-SAR (only a single scatterer physically located in the image).

29

(a)   (b)
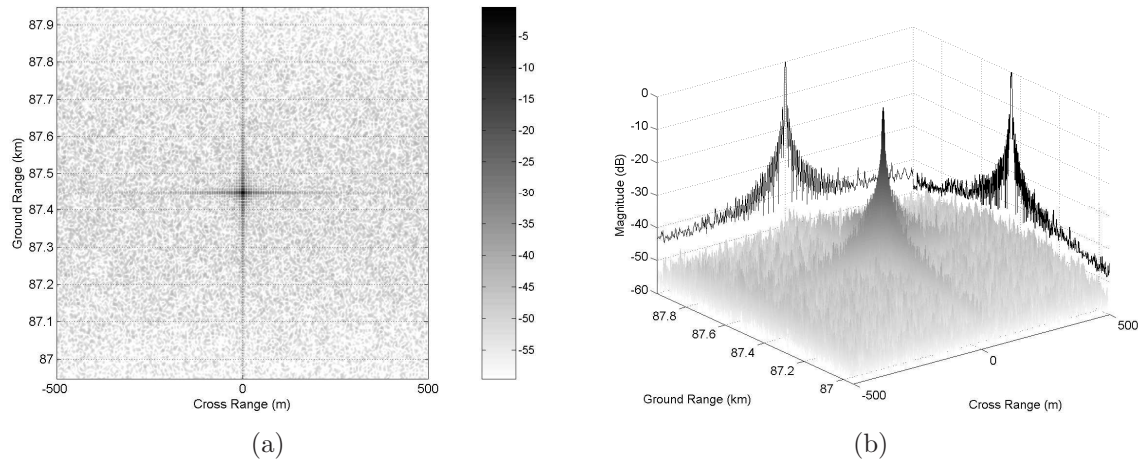
Figure 2.10:   (a) SAR image generated using RSF for $v_a = 100$ m/s with 60 dB dynamic range. The noisy background is a result of the noise-like ambiguity function of a single RSF waveform and incomplete cancellation of aliased scatterers. Coherent combination of many RSF waveforms pushes the noise floor down and enables cancellation of scatterers located at multiples of the PRF in Doppler.
(b) Surface plot showing the relative amplitudes of the primary and aliased targets. The maximum values along ground range and cross range are projected onto the walls. The background limits dynamic range to approximately -45 dB.

(a)   (b)
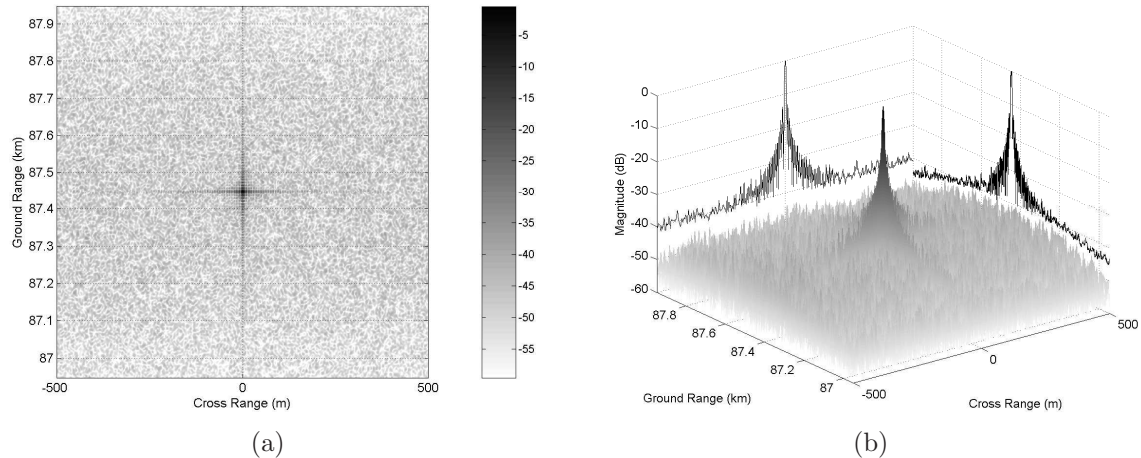
Figure 2.11:   (a) SAR image generated using RSF for $v_a = 200$ m/s with 60 dB dynamic range. At this velocity the aircraft travels twice as far between synthetic aperture locations, resulting in half as many RSF waveforms to combine. Additionally, there are twice as many scatterers which alias into the image at this aircraft velocity. The noisy background is more pronounced due both of these factors.
(b) Surface plot showing the relative amplitudes of the primary and aliased targets. The maximum values along ground range and cross range are projected onto the walls. The background limits dynamic range to approximately -40 dB.
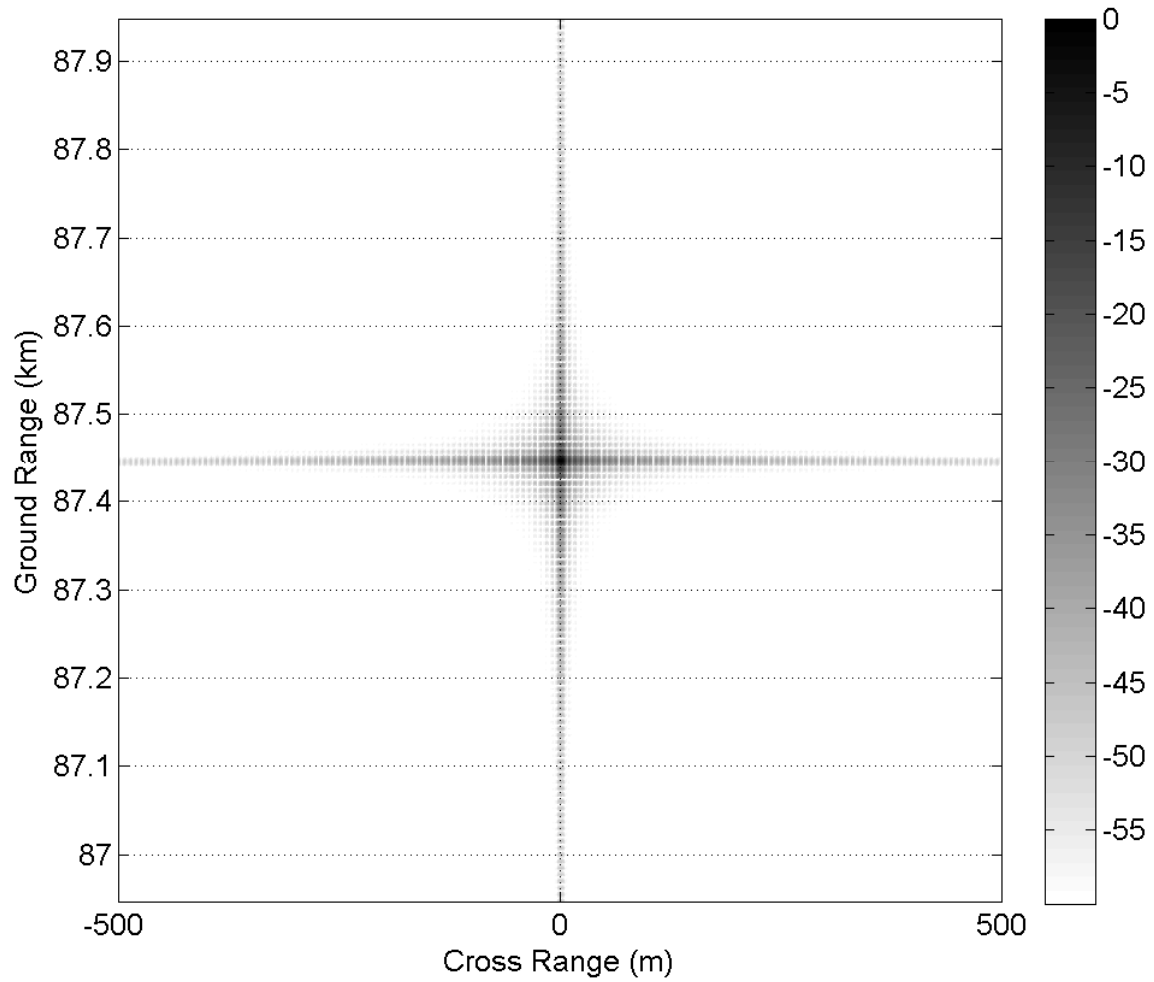
Figure 2.12: WA-SAR image of a single point scatterer using RSF for $v_a = 100$ m/s with 60 dB dynamic range. This image is characteristic of a point scatterer where sidelobes in range and cross range produce a cross pattern. No aliasing is present in this image and it will serve as a reference to compare with other images produced using RSF.

The normalized energy metric is computed for all images. The metric is generated by the following procedure:

1. Take the magnitude of the raw complex image data.

2. Normalize the data by dividing the image by its peak value.

3. Floor the data by discarding all values below the chosen floor.

4. Sum the squared magnitude of all pixels. This is the energy metric for the image.

5. Normalize the energy metric by dividing by the energy metric of an image generated of a scene where only the targets which are physically present in the image area are present (no scatterers to alias).

Once the normalized energy metric has been computed for all images it is possible to compare the aliased energy reduction capabilities of different waveforms. The percentage of aliased energy reduction is computed as follows:

1. Subtract 1 from the normalized energy metric of the reference image (most aliasing present). The result is the normalized energy of aliased targets only (The normalized energy of the desired targets is 1).

2. Subtract 1 from the normalized energy metric of the comparison image (less aliasing present).

3. Subtract the result of Step 2 from the result of Step 1.

4. Divide the result of Step 3 by the result of Step 1. This results in a ratio of the alias energy difference between the two images and the total aliased energy of the reference image. The ratio is the percentage of aliased energy present in the reference image which is not present in the comparison image.

The normalized energy metrics of both the LFM and RSF waveforms presented thus far can be seen in Table 2.3. The table also lists the percentage of aliased energy reduction from the LFM images.

Table 2.3: Normalized Energy Metrics for LFM, RSF and RSF-LFM

LFM Waveform		
Aircraft Velocity	Normalized Energy	% Aliased Energy Reduction from LFM
$v_a = 100$ m/s	3.45166	-
$v_a = 200$ m/s	6.57845	-
RSF Waveform		
Aircraft Velocity	Normalized Energy	% Aliased Energy Reduction from LFM
$v_a = 100$ m/s	1.10933	95.5407%
$v_a = 200$ m/s	1.26143	95.3135%
RSF-LFM Waveform		
Aircraft Velocity	Normalized Energy	% Aliased Energy Reduction from LFM
$v_a = 100$ m/s	1.10102	95.8797%
$v_a = 200$ m/s	1.23693	95.7528%

2.7 RSF-LFM Waveforms

RSF waveforms are effective in reducing the amount of aliased energy in WA-SAR. Additional improvement can be obtained with more uniform frequency coverage across the designated bandwidth. If the time-bandwidth region is uniformly filled then the approximation to Eqn. (2.26) improves and the nulling of aliased scatterers is improved. One approach which has been taken involves LFM modulation of the RSF subpulses (called RSF-LFM) [6]. The transmit signal becomes

$$s(t) = \frac{1}{\sqrt{\tau}} \sum_{n=0}^{N-1} \Pi \left(\frac{t - n\tau_s}{\tau_s} \right) \Re \left\{ e^{j2\pi f_n t} e^{j\pi \frac{Bt^2}{N\tau_s}} \right\}, \quad -\frac{\tau}{2} \leq t \leq \frac{\tau}{2} \qquad (2.28)$$

The time-frequency grid for RSF-LFM is shown in Fig. 2.13. It is evident from the time-frequency grid that the frequency across each subpulse is no longer constant, but linearly sweeps across the subpulse bandwidth.

The LFM coding on the RSF subpulses theoretically allows the time-bandwidth region to be filled more completely. As shown in [6] the short duration of each subpulse dominates the frequency content. The frequency content of a RSF-LFM subpulse
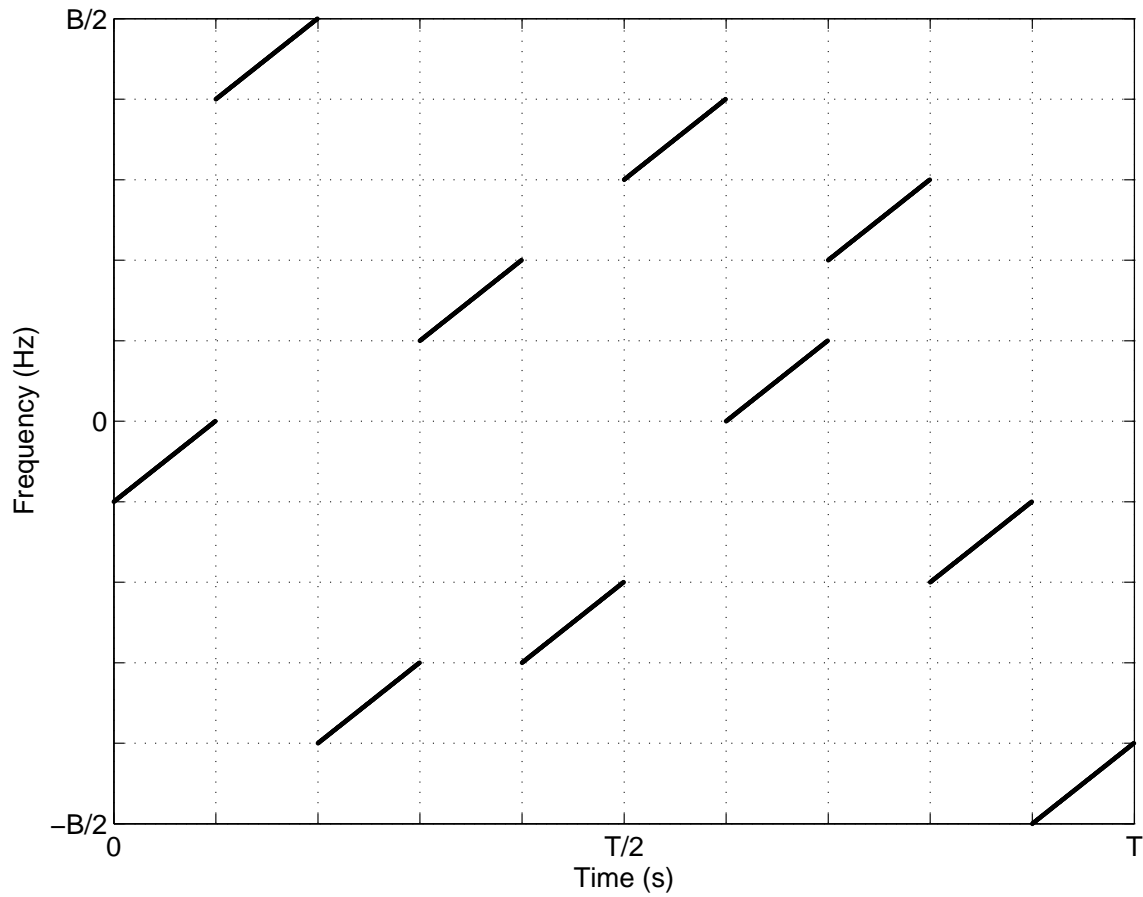
33

Figure 2.13:   RSF-LFM Time-Frequency Grid. Only 10 subpulses are used in order to illustrate the concept. The actual simulation uses 100 subpulses. In this figure, the actual frequency values which are transmitted during a particular subpulse are shown.
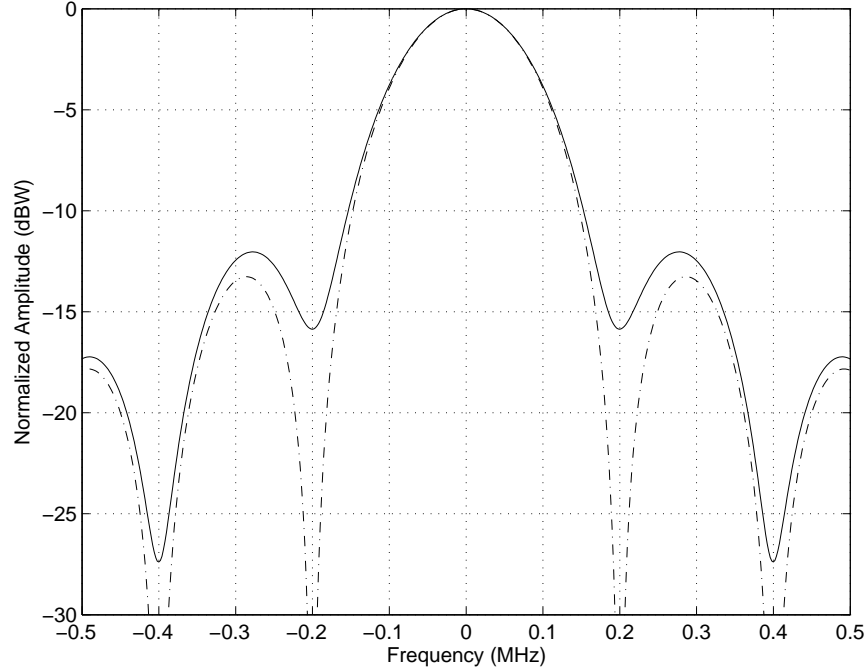
Figure 2.14: RSF-LFM subpulse (solid) versus RSF subpulse (dashed) frequency plot. During the short subpulse duration the frequency of a RSF-LFM subpulse increases linearly. Only a slight increase in the frequency content over a subpulse is present. The actual frequency content of the subpulse is attributed to the time duration of the subpulse.

compared to RSF is shown in Fig. 2.14. The frequency content of the entire waveform is almost identical to that pictured in Fig. 2.8. RSF-LFM waveforms provide only a marginal improvement over RSF [6].

WA-SAR images formed using the RSF-LFM waveform are shown in Figs. 2.15 and 2.16. The images are virtually identical to those formed using an uncoded RSF waveform. The normalized energy metrics for the RSF-LFM images are included in Table 2.3. The background level in Fig. 2.15 is approximately -45.3 dB while the background level in Fig. 2.16 is approximately -41.6 dB.

Better frequency coverage can be obtained from RSF-LFM by changing the underlying stepped frequency waveform by reducing the number of subpulses and changing the way the LFM is applied to the subpulses. This method changes the $B\tau = N^2$ relationship of the time frequency region to $B\tau > N^2$. Results for this type

35

(a)   (b)
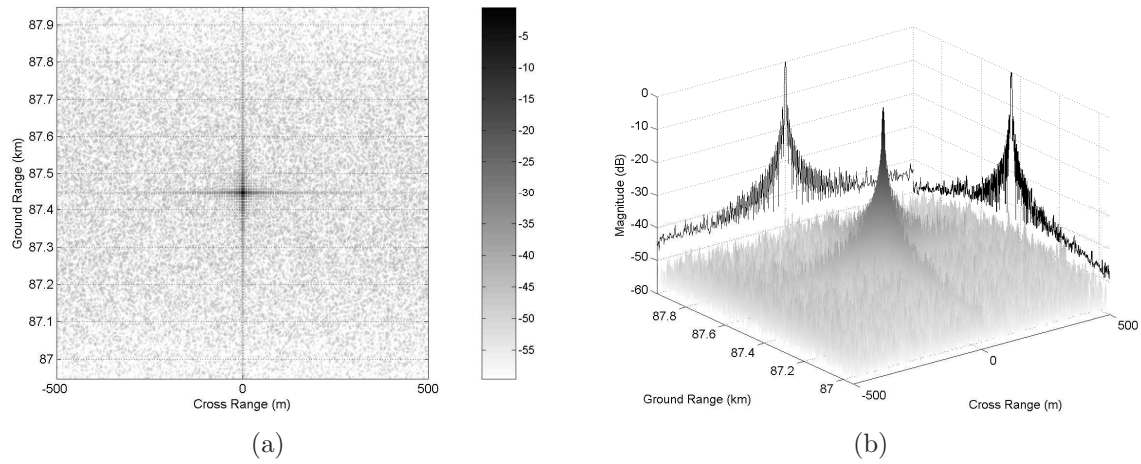
Figure 2.15:   (a) SAR image generated using RSF-LFM for $v_a = 100$ m/s with 60 dB dynamic range. Only a slight increase in frequency coverage on each subpulse results in no visible improvement in the WA-SAR image. Refer to Table 2.3 for the computed aliased energy reduction.
(b) Surface plot showing the relative amplitudes of the primary and aliased targets. The maximum values along ground range and cross range are projected onto the walls.

(a)   (b)
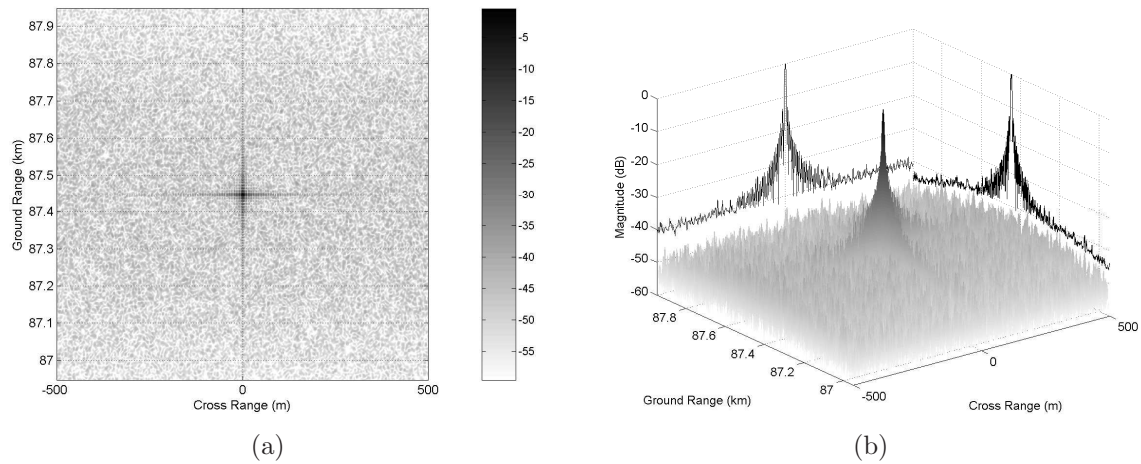
Figure 2.16:   (a) SAR image generated using RSF-LFM for $v_a = 200$ m/s with 60 dB dynamic range. Again, no visible improvement over an uncoded RSF waveform is visible. Refer to Table 2.3 for the computed aliased energy reduction.
(b) Surface plot showing the relative amplitudes of the primary and aliased targets. The maximum values along ground range and cross range are projected onto the walls.

of waveform modification do show some improvement in aliased energy reduction. Unfortunately, depending on the amount of aliased energy to be mitigated, an image may experience unexplained degradation due to clumping of aliased energy [6].

The current research effort examines phase modulation of the RSF subpulses as an alternative method of improving the frequency coverage of each RSF subpulse without changing the subpulse duration. Chapter III introduces the phase modulations and their application to RSF waveforms. Chapter IV examines WA-SAR images produced using the phase modulated RSF waveforms.

III. Phase Modulation applied to RSF Waveforms

As discussed in Section 2.7, Doppler alias mitigation improvement over the uncoded RSF waveform can be achieved if the time-bandwidth space is uniformly covered. An uncoded RSF waveform subpulse covers its designated portion of the spectrum as illustrated in Fig. 2.7. One way of accomplishing more uniform coverage is modulation of the individual RSF subpulses. This chapter will introduce several phase modulation techniques which will be applied to RSF waveforms. In addition, several improvements to the simulation model have been incorporated which increase the fidelity of the simulations. These improvements include a realistic antenna pattern and correct modeling of time overlapped waveforms on receive. Chapter IV will show the results of using the phase modulated waveforms in the WA-SAR scenario.

Phase modulation is commonly used in radar for pulse compression and in communications for direct-sequence spread spectrum applications. Phase modulations may be classified as either binary phase or polyphase. Binary phase codings modulate phase by either 0 or 180 degrees. Polyphase systems allow additional combinations of phase shifts beyond those used for binary phase.

The phase modulations examined in this research are Barker, Frank and P4 codes. Each of these will be examined in more detail in this chapter.

3.1 Barker Codes

Barker codes are one type of binary phase modulation which have the unique property of having equal autocorrelation sidelobe levels [9]. Barker codes exist for various lengths of up to a maximum of 13. The length 13 Barker code is

$$[+ + + + + - - + + - + - +] \tag{3.1}$$

where a $+$ indicates zero phase shift and $-$ indicates a phase shift of $180°$. The length 13 Barker code's autocorrelation function has time sidelobes that are -22.3 dB down from the peak [9].

In order to apply the length 13 Barker code to a RSF waveform, each of the N subpulses of Eqn. (2.24) is divided further into 13 sub-subpulses. In the model used for this research, each RSF subpulse is comprised of 200 time samples. Dividing this into 13 sub-subpulses results in 15 samples per sub-subpulse. The remaining 5 samples at the end of the subpulse are grouped into the last sub-subpulse, resulting in it having 20 time samples. The phase of each sub-subpulse is coded according to Eqn. (3.1).

The effect of subdividing the subpulse into sub-subpulses results in frequency spreading related to the time duration of the sub-subpulses. The frequency coverage of a Barker coded subpulse is compared to an uncoded RSF subpulse in Fig. 3.1. The mainlobe frequency response of the RSF-Barker coded subpulse is approximately 13 times wider than the RSF subpulse. While the frequency coverage of the subpulse is increased, it is obvious that sidelobe levels have increased substantially and do not taper off nearly as much as the RSF subpulse sidelobe levels.

The entire RSF-Barker waveform frequency coverage is shown in Fig. 3.2. Notice the frequency coverage adequately covers the designated bandwidth. Unfortunately, outside of the specified 20 MHz bandwidth (see Table 2.2) there is leakage into neighboring frequencies. The frequency magnitude 5 MHz outside of the waveform's bandwidth is approximately 12.2 dB higher than uncoded RSF. This could be undesirable if other nearby systems use frequencies near that of the WA-SAR system. Additionally, actual systems limit receiver bandwidth. Such bandlimiting will produce increased time-sidelobes and SNR loss [3].

3.2   Frank Codes

Frank codes are polyphase codes where the phase shifts are not limited to 0 and 180 degrees. The phase shifts of a length M^2 Frank code are defined by a $M \times M$

39

Figure 3.1: This figure shows the Fourier transform of a single Barker coded RSF subpulse (solid) versus the Fourier transform of an uncoded RSF subpulse (dashed). A length 13 Barker code applied to a RSF waveform results in each subpulse spreading in frequency and significantly higher sidelobe levels. The frequency coverage of the entire waveform (N subpulses combined) is shown in Fig. 3.2.
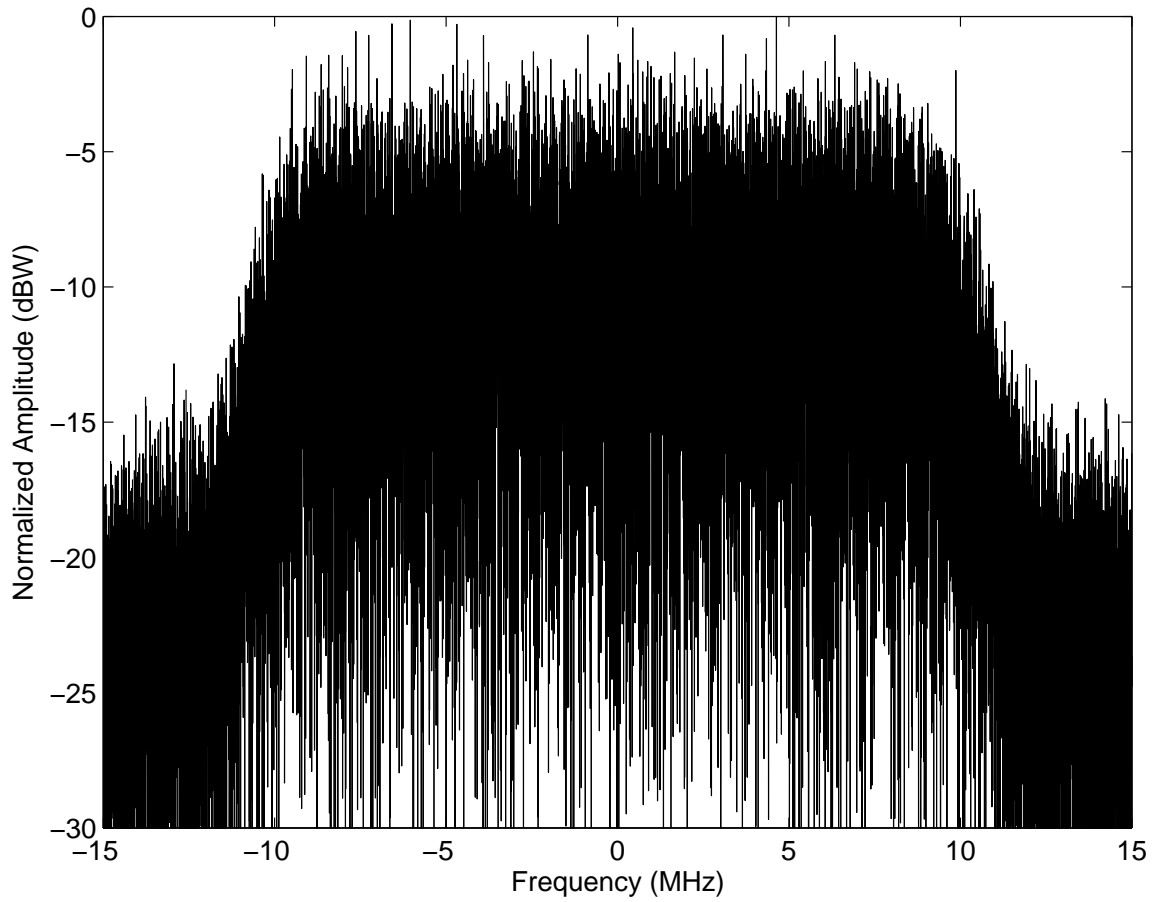
Figure 3.2:   RSF-Barker coded waveform frequency plot. A length 13 barker code applied to a RSF waveform results in undesired frequency content extending beyond the specified 20 MHz bandwidth of the signal.

matrix [9]

$$\frac{2\pi}{M} \times \begin{bmatrix} 0 & 0 & 0 & \cdots & 0 \\ 0 & 1 & 2 & \cdots & (M-1) \\ 0 & 2 & 4 & \cdots & 2(M-1) \\ 0 & 3 & 6 & \cdots & 3(M-1) \\ \vdots & \vdots & \vdots & \ddots & \vdots \\ 0 & (M-1) & 2(M-1) & \cdots & (M-1)^2 \end{bmatrix} \qquad (3.2)$$

The phases of the length M^2 code are taken starting at the top row, left to right, with each successive row following in like manner.

The Frank codes are applied to each of the N RSF subpulses of Eqn. (2.24) in a similar manner as they were applied for the RSF-Barker waveform. Each subpulse of the RSF waveform is divided further into M^2 sub-subpulses, where M^2 represents the length of the code. For a RSF subpulse comprised of 200 time samples a length 25 Frank code will have sub-subpulses that are 8 samples long. The phase of each sub-subpulse is coded according to Eqn. (3.2).

The subpulse frequency content for a RSF-Frank coded subpulse is shown in Fig. 3.3. The mainlobe frequency response of the RSF-Frank coded subpulse is approximately 25 times wider than that of the RSF subpulse. The frequency coverage of each subpulse is increased, and sidelobe levels have increased similarly to the RSF-Barker coded subpulses.

The entire RSF-Frank coded waveform frequency coverage is shown in Fig. 3.4. Notice that the frequency coverage adequately covers the designated bandwidth. Unfortunately, outside of the 20 MHz bandwidth there is significant leakage into neighboring frequencies. The frequency magnitude 5 MHz outside of the waveform's bandwidth is approximately -14.5 dB (an increase of 14.2 dB over uncoded RSF). This could be undesirable if other nearby systems use frequencies near that of the WA-SAR system. Additionally, in actual systems receiver bandlimiting will produce increased time-sidelobes and SNR loss [3].
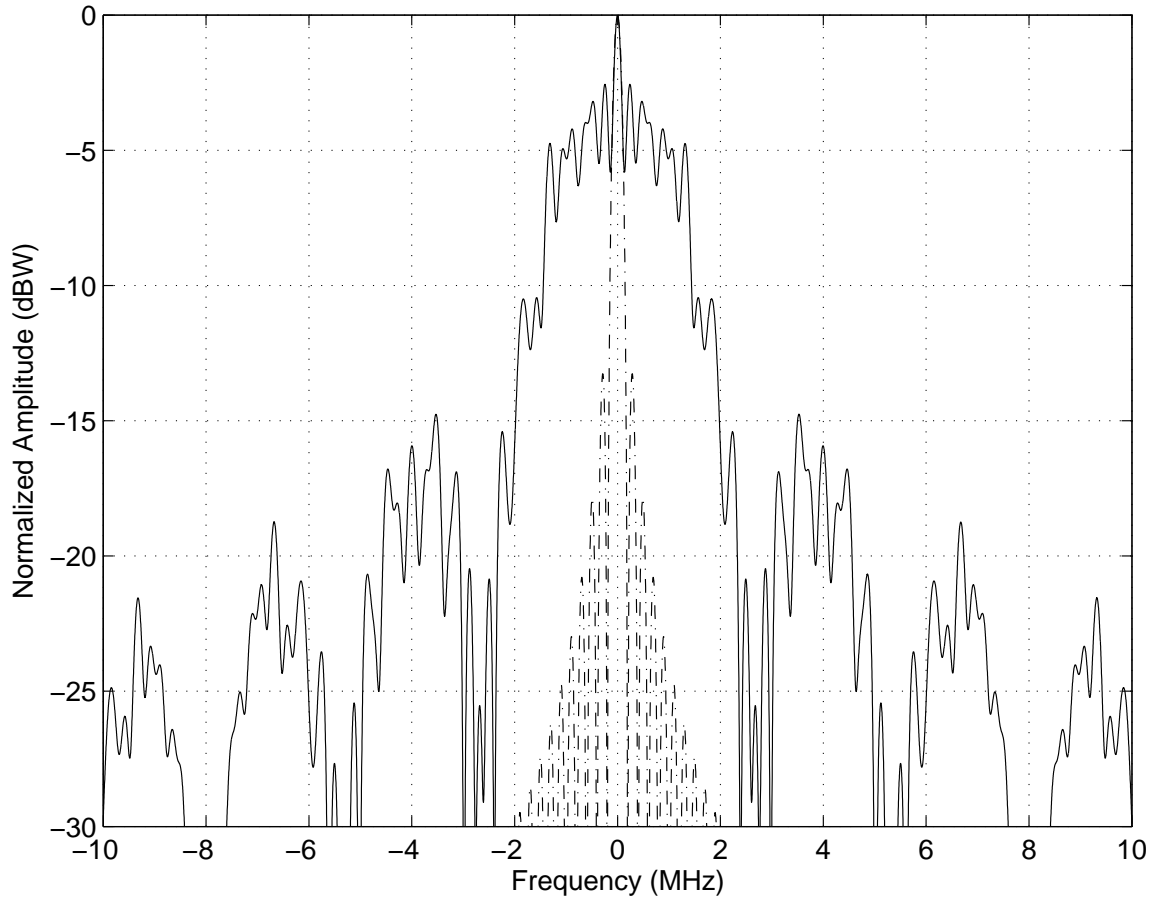
42

Figure 3.3: This figure shows the Fourier transform of a single Frank coded RSF subpulse (solid) versus the Fourier transform of an uncoded RSF subpulse (dashed). A length 25 Frank code applied to a RSF waveform results in each subpulse spreading in frequency and significantly higher sidelobe levels. The frequency coverage of the entire waveform (N subpulses combined) is shown in Fig. 3.4.

43
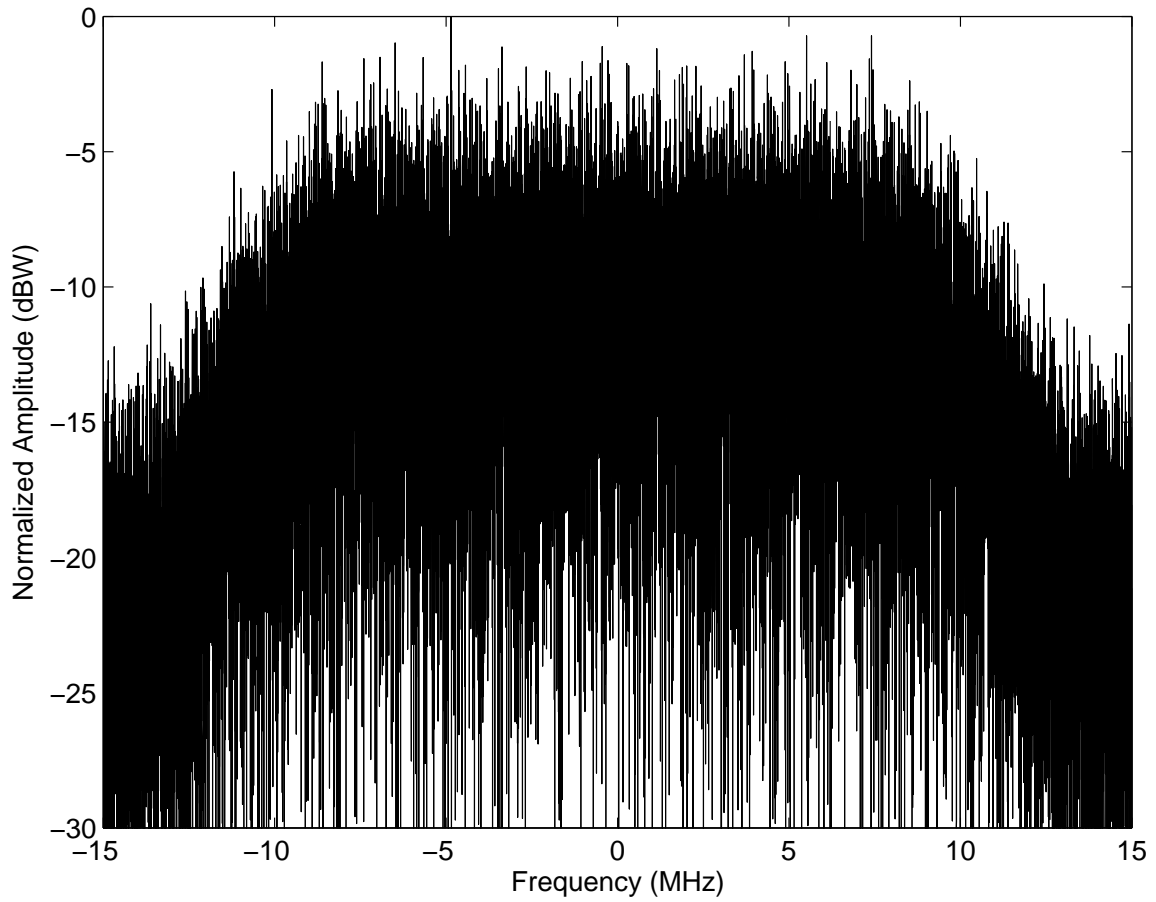
Figure 3.4:   RSF-Frank coded waveform frequency plot. A length 25 Frank code
applied to a RSF waveform results in frequency content extending beyond the specified
20 MHz bandwidth of the signal.

3.3 P4 Codes

P4 codes are variants of the Frank polyphase codes which can be made any length. The ith phase in a P4 code of length N is described as [3]

$$\phi_i = \left[\frac{\pi(i-1)^2}{N} \right] - \pi(i-1), \qquad 1 \le i \le N \tag{3.3}$$

The P4 codes are applied to each of the N RSF subpulses in Eqn. (2.24) just as they were applied for the RSF-Frank waveform. Each subpulse of the RSF waveform is divided further into M sub-subpulses, where M represents the length of the code. For a RSF subpulse comprised of 200 time samples a length 25 P4 code will have sub-subpulses that are 8 samples long. The phase of each sub-subpulse is coded according to Eqn. (3.3).

The subpulse frequency content for a RSF-P4 coded subpulse is shown in Fig. 3.5. The mainlobe frequency response of the RSF-P4 coded subpulse is approximately 25 times wider than that of the RSF subpulse. The frequency coverage of each subpulse is increased, and sidelobe levels have increased similarly to the RSF-Barker and RSF-Frank coded subpulses. The frequency coverage of each subpulse is increased, and it is obvious that sidelobe levels have increased substantially and do not taper off nearly as much as the RSF subpulse sidelobe levels.

The entire RSF-P4 coded waveform frequency coverage is shown in Fig. 3.6. Notice that the frequency coverage adequately covers the designated bandwidth with no obvious gaps. Unfortunately, outside of the 20 MHz bandwidth there is significant leakage into neighboring frequencies. The frequency magnitude 5 MHz outside of the waveform's bandwidth is approximately -12.9 dB (an increase of 15.8 dB over uncoded RSF). This could be undesirable if other nearby systems use frequencies near that of the WA-SAR system. Additionally, in actual systems receiver bandlimiting will produce increased time-sidelobes and SNR loss [3].
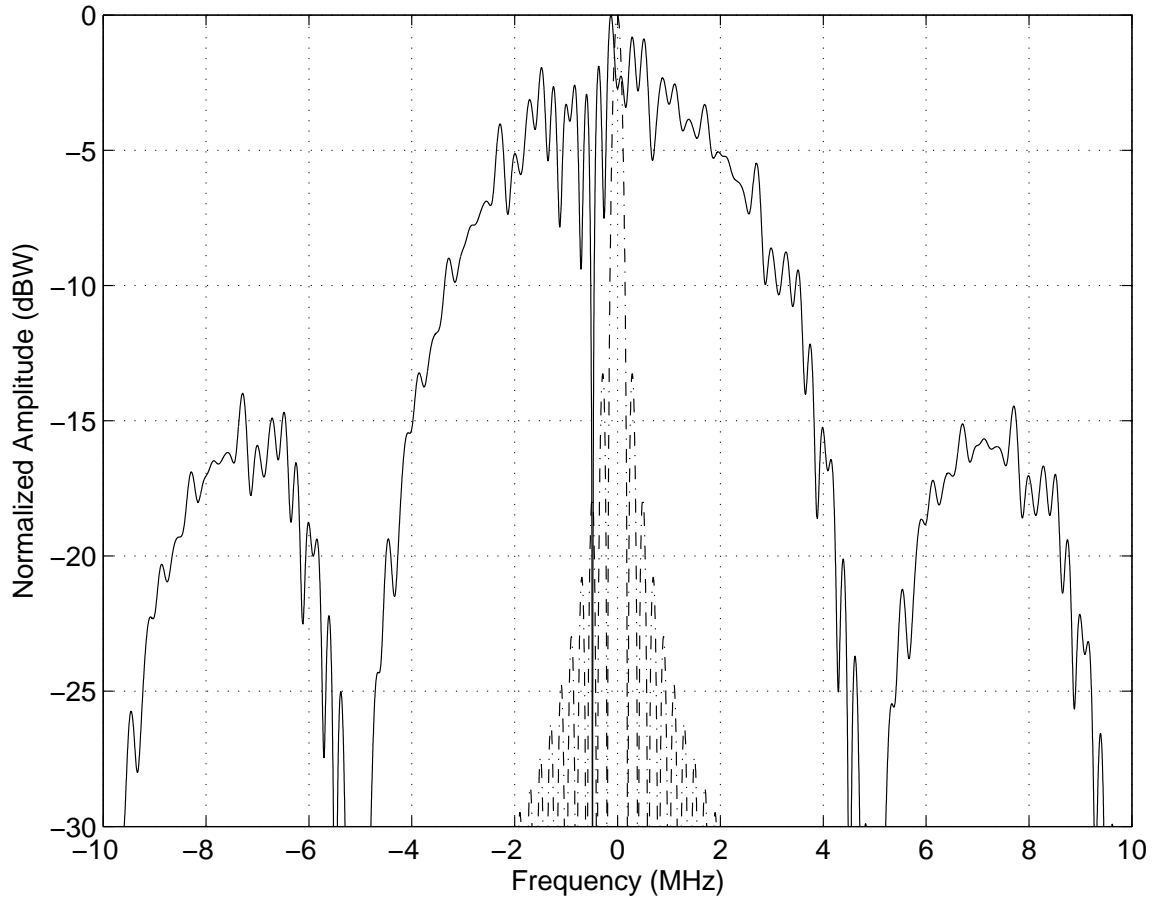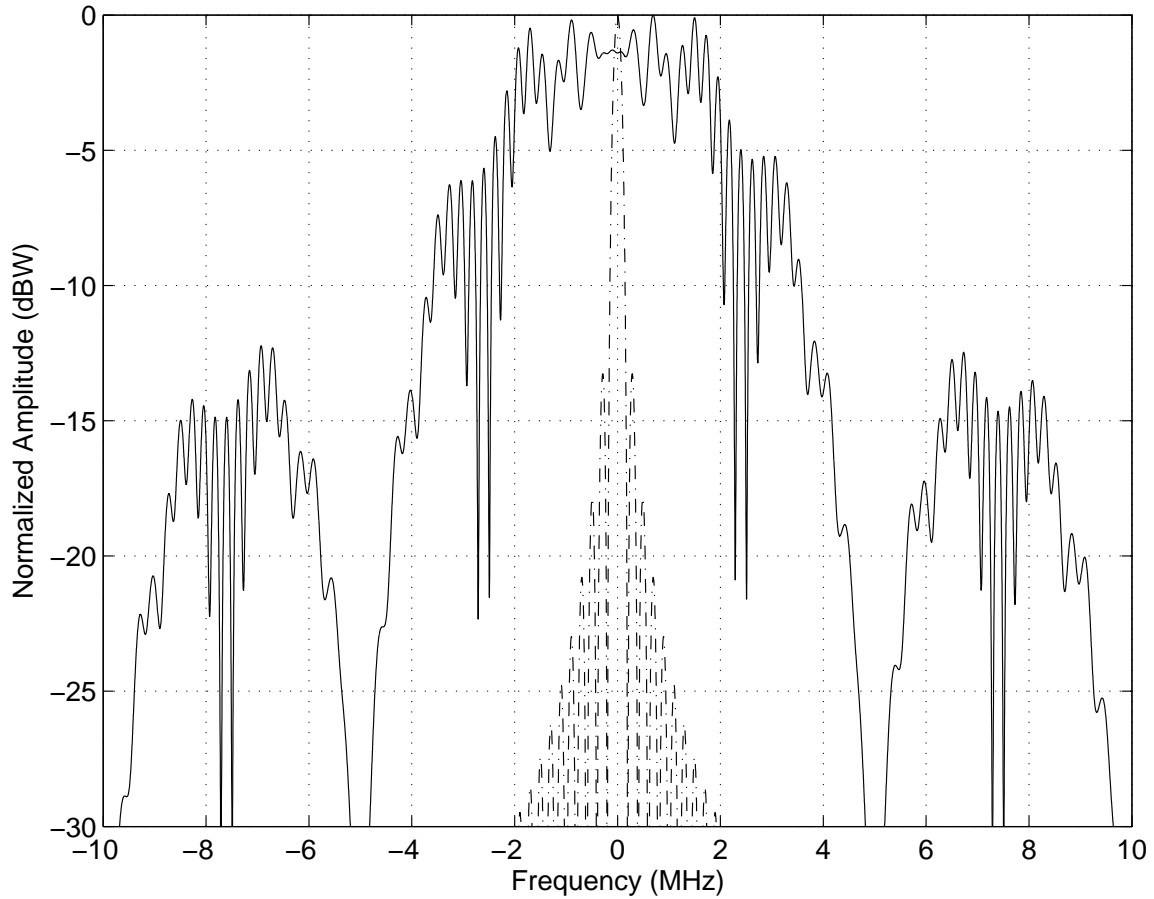
Figure 3.5: This figure shows the Fourier transform of a single P4 coded RSF subpulse (solid) versus the Fourier transform of an uncoded RSF subpulse (dashed). A length 25 P4 code applied to a RSF waveform results in each subpulse spreading in frequency and significantly higher sidelobe levels. The frequency coverage of the entire waveform (N subpulses combined) is shown in Fig. 3.6.

Figure 3.6: RSF-P4 coded waveform frequency plot. A length 25 P4 code applied to a RSF waveform results in frequency content extending beyond the specified 20 MHz bandwidth of the signal.

Three new phase coded RSF waveforms have been presented so far in this chapter. Using the model improvements which will be discussed next, the phase coded waveforms will be used to form WA-SAR images in Chapter IV.

3.4 Model Improvements

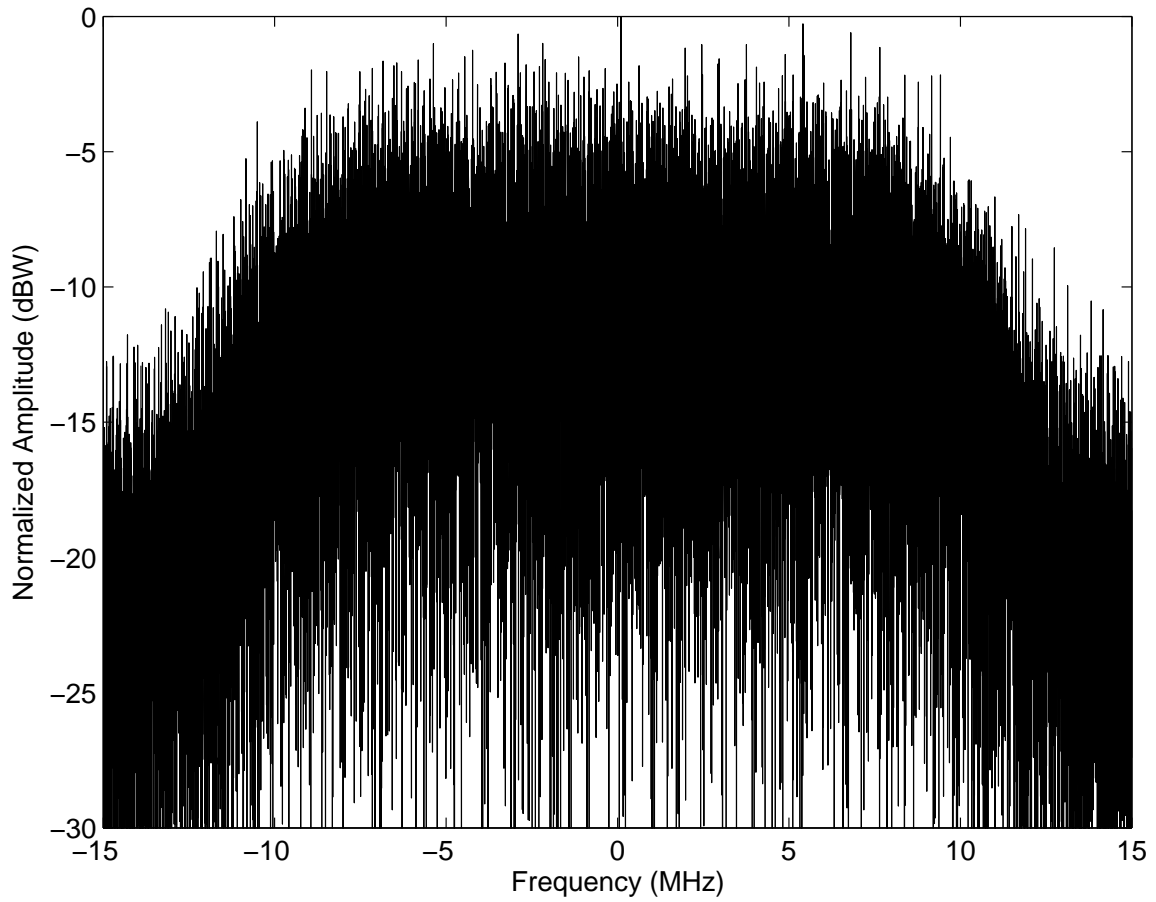Previous research [4, 6] has shown that RSF waveforms are effective in mitigating Doppler aliasing in WA-SAR. The models which were used in that research incorporated various assumptions. As part of the current research effort, several of those assumptions were removed.

3.4.1 Antenna Pattern. Previous models specified a uniform antenna pattern with an azimuth mask to limit the viewing angle to $\pm 45°$. The model used in the present research employs a vertical, linear array to simulate a single element antenna with wide azimuthal beamwidth and relatively narrow elevation beamwidth. Specifying a physical antenna pattern allows for more realistic simulations. The antenna pattern affects the amplitude of target returns and allows the amplitude to vary slightly over the length of the synthetic aperture as the angles to the target change.

The implemented antenna pattern's azimuth and elevation gains are shown in Fig. 3.7. The antenna pattern is steered slightly down (approximately $-2°$) in elevation in order to provide maximum response in elevation over the ranges of interest (see Table 2.2). The array elements are spaced uniformly one half-wavelength apart. The linear array is implemented only to generate the desired elevation pattern. The actual physical antenna is assumed to generate a similar pattern using only a single element.

3.4.2 Pulse Overlap due to Continuous Wave Operation. RSF waveforms are able to null out aliased targets if the Pulse Repetition Frequency (PRF) is equal to $1/\tau$ (see Section 2.6). This requirement causes Continuous Wave (CW) operation where a waveform is transmitted every τ seconds. As a pulse travels out over the
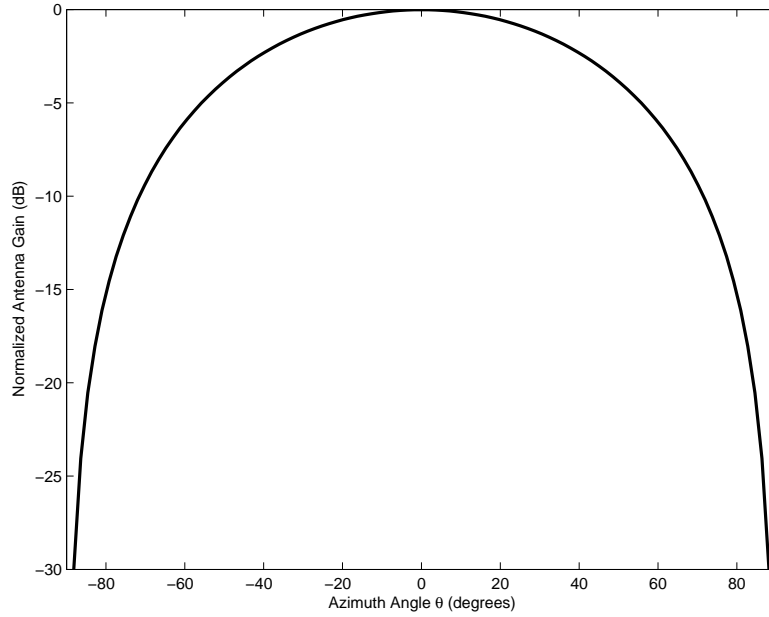
(a)
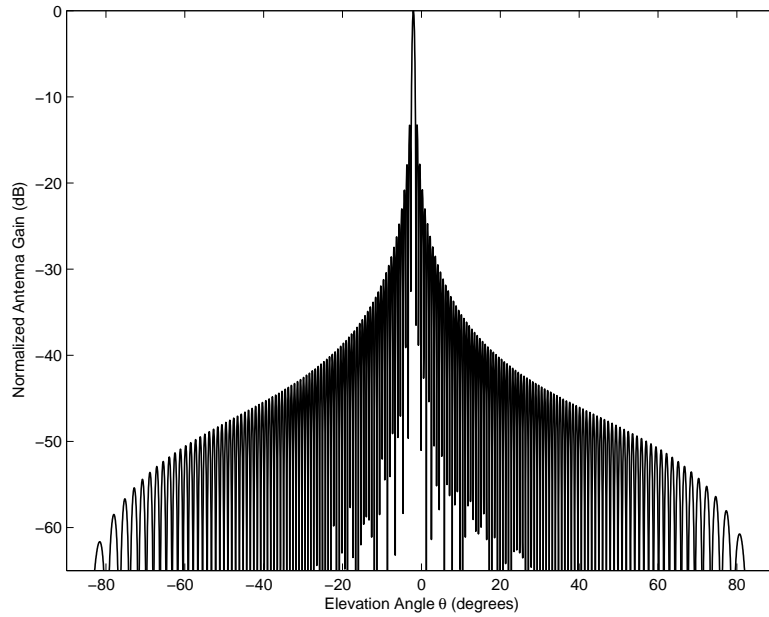
(b)

Figure 3.7: (a) Antenna gain pattern in azimuth. The -3 dB azimuth beamwidth is 90°.
(b) Antenna gain pattern in elevation. The elevation -3 dB beamwidth is approximately 0.6°. In elevation the beam is steered downward by approximately −2° so that the -3 dB elevation beamwidth is centered on the ranges of interest (75 km to 100 km).
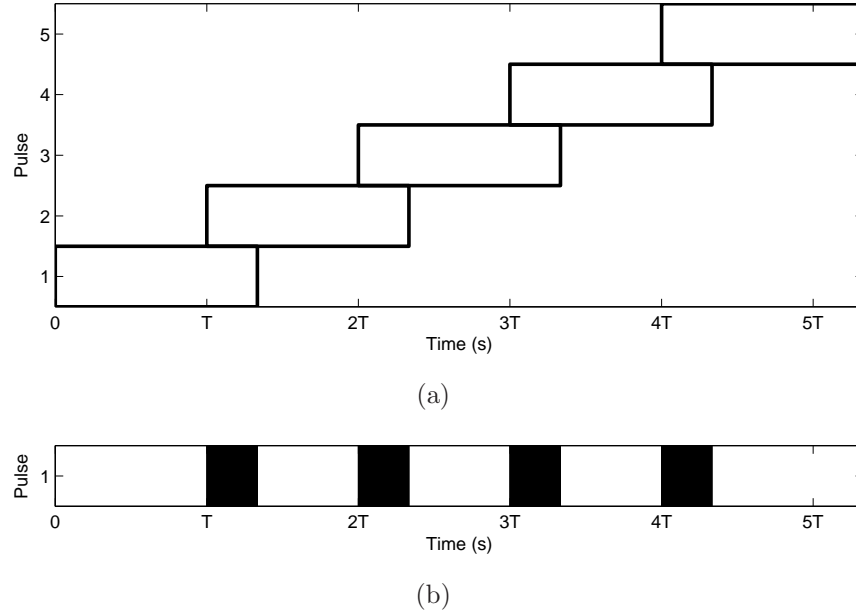
49

Figure 3.8: (a) Illustration of pulse overlap due to CW operation. Transmission of pulses occurs every T seconds but the received pulse is longer due to reflections from different parts of the scene.
(b) The overall received signal is continuous. Shaded areas represent portions of the signal with containing parts of 2 distinct waveforms.

ranges of interest, the signal reflects off each target in the scene and travels back towards the radar. The return from each scatterer is received and summed with other returns based on the round trip time to each scatterer. The composite return from all scatterers is a summation of the individual returns from each scatterer in the scene. The amount of time needed to receive the composite return $\tau + 2R_p/c$ where R_p is the distance across the ranges of interest. It takes longer to receive the composite return signal than it does to transmit each individual pulse.

The extra time needed to receive returns results in a partial overlap of different transmit waveforms. For example, a return from a target at the far edge of the scene will be partially overlapped by the next pulse's return from the near edge of the scene. This is illustrated in Fig. 3.8. The model developed for this research incorporates the overlap.

50

The method of processing returns dictates a different matched filter be used on each pulse because each pulse uses a unique frequency ordering. In order to accomplish this, segments of the overlapped received signal corresponding to a given transmit waveform are extracted and matched filtered. In general both ends of the received waveform sent through the matched filter are corrupted by the overlap of the previous and next waveforms. Therefore the range profiles which are generated have higher range sidelobes generated due to mismatched filtering. The effects are not noticeable in the images produced in this research. This is primarily due to the fact that the images are formed using ranges which lie in the uncorrupted region of each pulse return. Previous research also formed images of targets near the center of the range extent of the scene. It is likely that images formed near the edges of the scene would exhibit degradation due to the cross-correlation effects.

3.5 Summary

By applying phase coding to the subpulses of a RSF waveform, the frequency coverage of each subpulse is increased. The increased frequency coverage of the subpulses results in more uniform filling of the time-bandwidth region of the RSF waveform.

Incorporation of a realistic antenna pattern and correct overlapping of pulses allows the simulation to more accurately model real world effects. Using a model incorporating such improvements, the RSF-Barker, RSF-Frank and RSF-P4 phase coded waveforms introduced in this chapter are used to generate WA-SAR images in Chapter IV.

IV.   Results of Using Phase Coded RSF Waveforms

Chapter III introduced three new phase coded Random Stepped Frequency (RSF) waveforms. These waveforms have improved subpulse frequency coverage due to the phase coding of each subpulse. Each of these waveforms will now be used to form Wide-Angle SAR (WA-SAR) images. The images formed using the phase coded waveforms will be compared to the images formed in Chapter II through the use of the normalized energy metric introduced in Section 2.6.2.

For comparison with the new images, the WA-SAR images formed using the Linear Frequency Modulation (LFM) waveform (Figs. 2.4(a) and 2.5(a)) are presented again in Fig. 4.1. Also, the images produced using the uncoded RSF waveform (Figs. 2.10(a) and 2.11(a)) are shown in Fig. 4.2.

4.1   RSF-Barker Coded Waveforms

The RSF-Barker coded waveform introduced in Section 3.1 is set as $s(t)$ in the WA-SAR model and an image is formed using the Convolution/Back-Projection (CBP) algorithm. The image formed for an aircraft velocity of 100 m/s is shown in Fig. 4.3(a). When compared with the LFM image in Fig. 4.1(a), it is clear that the aliasing present in the LFM image has been mitigated by using the RSF-Barker coded waveform. Additionally, comparison with the RSF waveform in Figure 4.2(a) shows that the background is reduced. The noise-like background appears to have relatively uniform coverage in cross range and be confined to ranges where the other scatterers in the scene are located. Figure 4.3(b) shows the image with pixel amplitude represented as height. The aliased energy which remains in this image is lower amplitude than the point scatterer sidelobes. The background level in Fig. 4.3 is approximately -53.5 dB.

Figure 4.4 shows that, with the aircraft velocity at 200 m/s, the aliased scatterers are not present. The noise-like background is reduced when compared to the RSF image in Fig. 4.2(b). The noise-like background is again confined to ranges where other scatterers exist in the scene. The presence of additional aliasing energy at this aircraft velocity increases the amplitude of the background compared to Fig. 4.3(a).
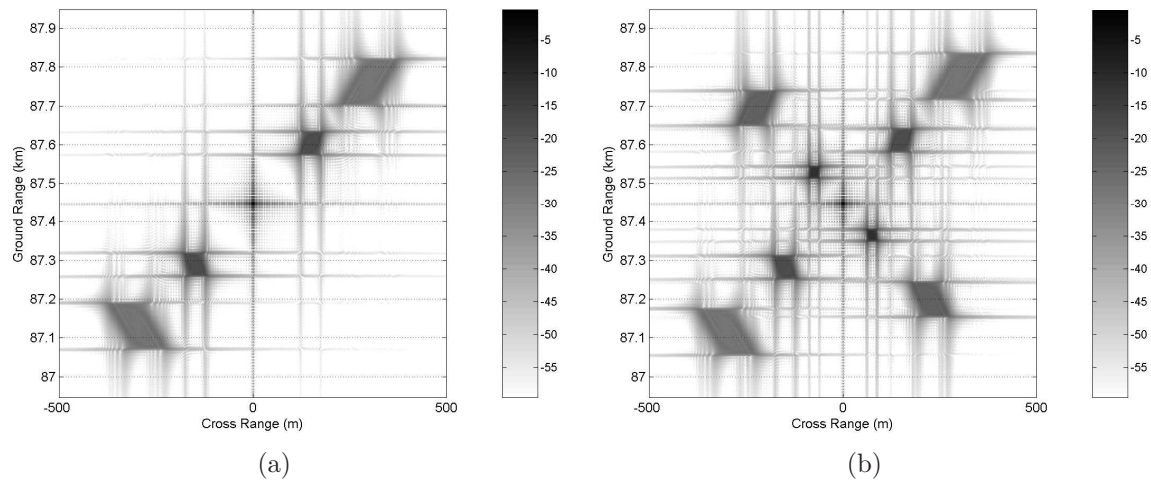
Figure 4.1:   (a) SAR image generated using a LFM waveform for $v_a = 100$ m/s with 60 dB dynamic range.
(b) SAR image generated using a LFM waveform for $v_a = 200$ m/s with 60 dB dynamic range. The LFM images are used to compare with similar images formed using phase coded waveforms to illustrate the effectiveness of the new waveforms in mitigating Doppler aliasing.
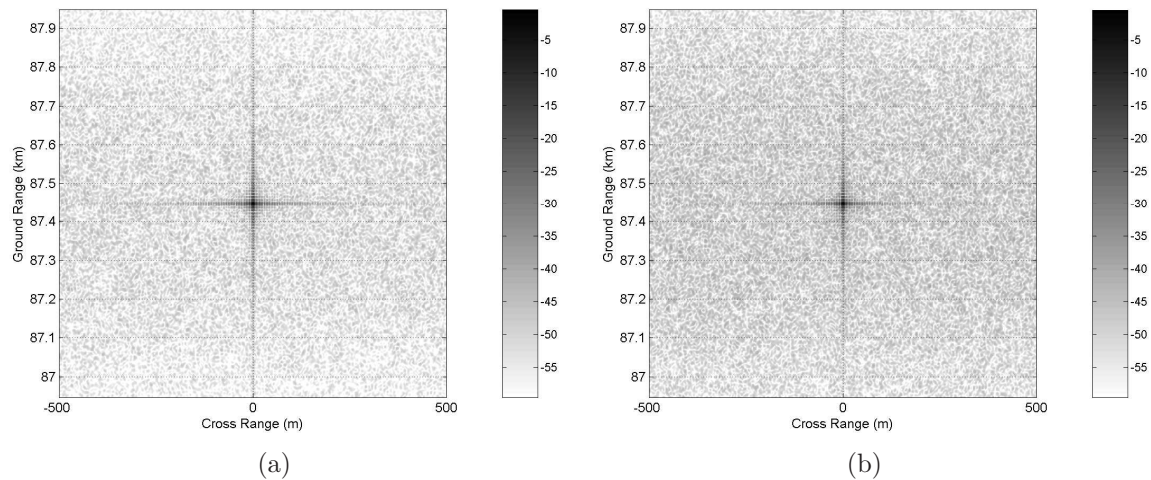

Figure 4.2:   (a) SAR image generated using a RSF waveform for $v_a = 100$ m/s with 60 dB dynamic range.
(b) SAR image generated using a RSF waveform for $v_a = 200$ m/s with 60 dB dynamic range. The RSF images are used to compare with similar images formed using phase coded waveforms to illustrate the additional effectiveness of the new waveforms in mitigating Doppler aliasing.

Figure 4.4(b) shows the image with pixel amplitude represented as height. The aliased energy which remains in this image is lower amplitude than the point scatterer side-lobes. The background level in Fig. 4.4 is approximately -50.7 dB.

4.2 RSF-Frank Coded Waveforms

The RSF-Frank coded waveform which was introduced in Section 3.2 is set as $s(t)$ in the WA-SAR model and an image is formed using the CBP algorithm. The image formed for an aircraft velocity of 100 m/s is shown in Fig. 4.5(a). When compared with the LFM image in Fig. 4.1(a), it is clear that the aliasing present in the LFM image has been mitigated by using the RSF-Frank coded waveform. Additionally, comparison with the RSF waveform in Fig. 4.2(a) shows that the noise-like background is almost completely suppressed. The background again appears confined to ranges where the other scatterers in the scene are located indicating that it is due to the other targets. Figure 4.5(b) shows the image with pixel amplitude represented as height. The aliased energy which remains in this image is lower amplitude than the point scatterer sidelobes. The background level in Fig. 4.5 is approximately -56.8 dB.

Figure 4.6 shows that, with the aircraft velocity at 200 m/s, the aliased scatterers are not present. The noise-like background is reduced when compared to the RSF image in Fig. 4.2(b). The noise-like background is again confined to ranges where other scatterers exist in the scene. The presence of additional aliasing energy at this aircraft velocity increases the amplitude of the background compared to Fig. 4.5. The background level in Fig. 4.6 is approximately -53.9 dB.

4.3 RSF-P4 Coded Waveforms

The RSF-P4 coded waveform which was introduced in Section 3.3 is set as $s(t)$ in the WA-SAR model and an image is formed using the CBP algorithm. The image formed for an aircraft velocity of 100 m/s is shown in Fig. 4.7. When compared with the LFM image in Fig. 4.1(a) , it is clear that the aliasing present in the LFM image has been mitigated by using the RSF-P4 coded waveform. Additionally, comparison

54

Figure 4.3: (a) SAR image generated using RSF-Barker for $v_a = 100$ m/s with 60 dB dynamic range.
(b) Surface plot showing the relative amplitudes of the primary and aliased targets. The maximum values along ground range and cross range are projected onto the walls.
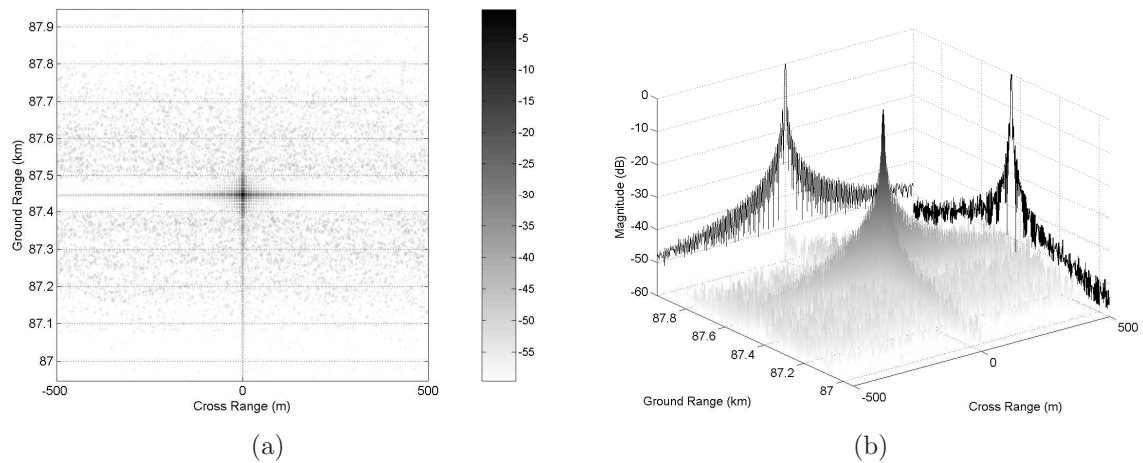
Figure 4.4: (a) SAR image generated using RSF-Barker for $v_a = 200$ m/s with 60 dB dynamic range.
(b) Surface plot showing the relative amplitudes of the primary and aliased targets. The maximum values along ground range and cross range are projected onto the walls.
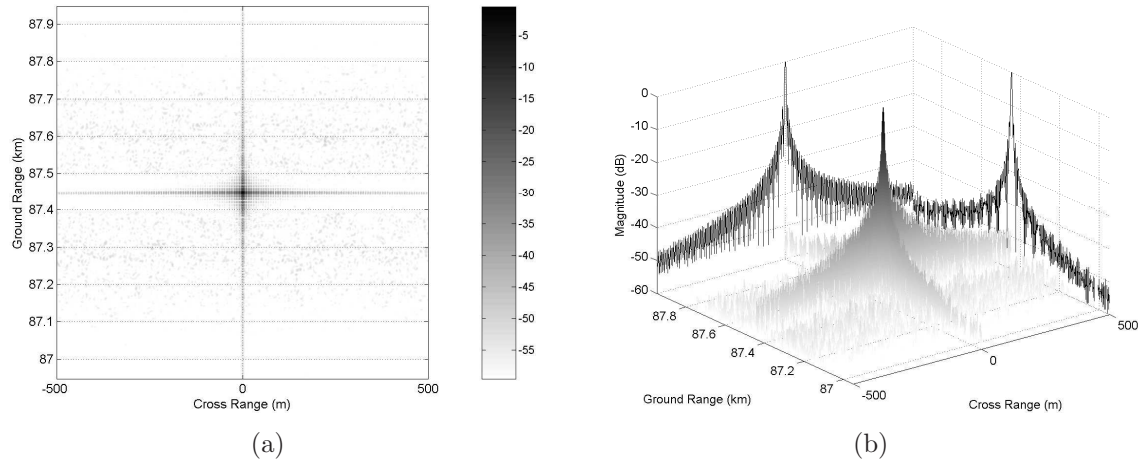
Figure 4.5:   (a) SAR image generated using RSF-Frank for $v_a = 100$ m/s with 60 dB dynamic range.
(b) Surface plot showing the relative amplitudes of the primary and aliased targets. The maximum values along ground range and cross range are projected onto the walls.

Figure 4.6:   (a) SAR image generated using RSF-Frank for $v_a = 200$ m/s with 60 dB dynamic range.
(b) Surface plot showing the relative amplitudes of the primary and aliased targets. The maximum values along ground range and cross range are projected onto the walls.
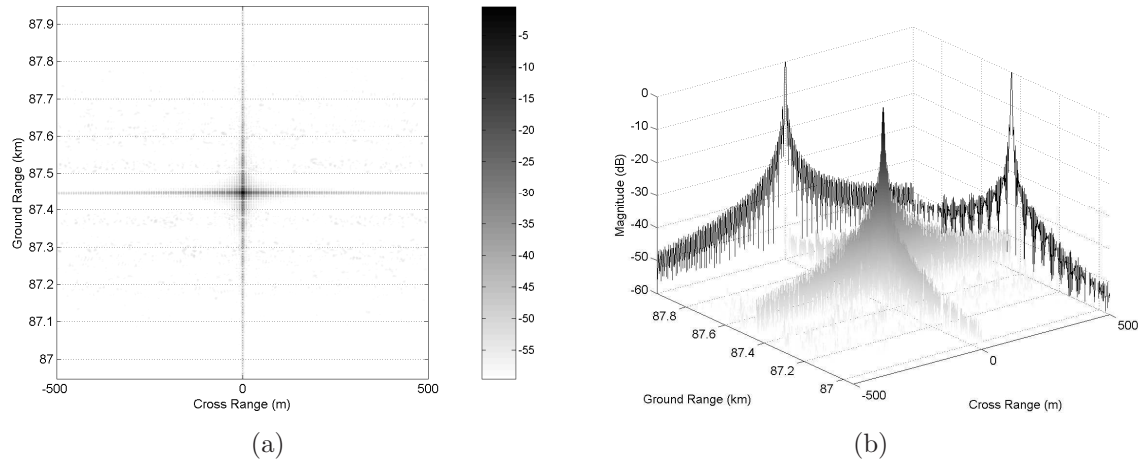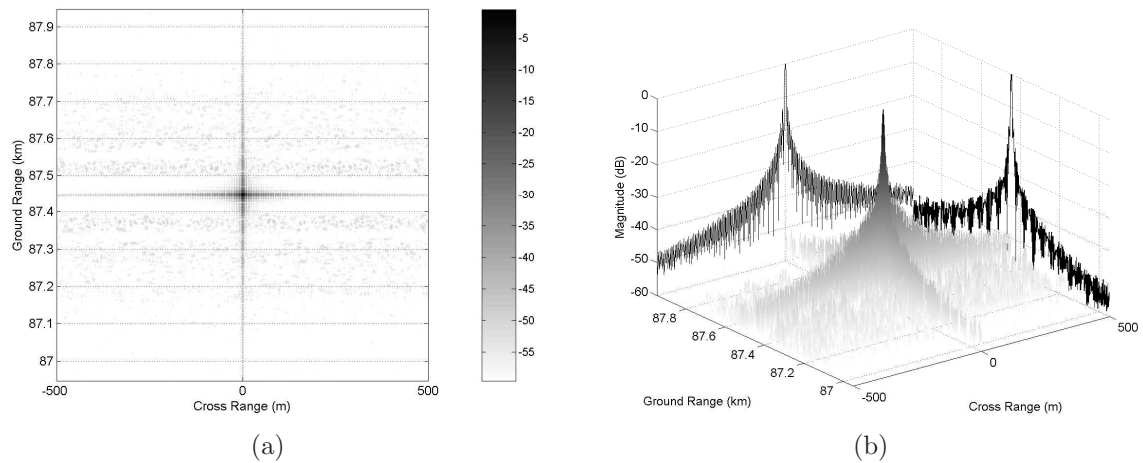
56

with the RSF waveform in Fig. 4.2(a) shows that the noise-like background is almost completely suppressed. The background again appears confined to ranges where the other scatterers in the scene are located indicating that it is due to the other targets. The background level in Fig. 4.7 is approximately -56.2 dB.

Figure 4.8 shows that, with the aircraft velocity at 200 m/s, the aliased scatterers are not present. The noise-like background is reduced when compared to the RSF image in Fig 4.2(b). The background is again confined to ranges where other scatterers exist in the scene. The presence of additional aliasing energy at this aircraft velocity increases the amplitude of the background compared to Fig. 4.7. In almost all respects, the RSF-P4 images are virtually indistinguishable from the RSF-Frank images. The background level in Fig. 4.8 is approximately -53.7 dB.

4.4   *Normalized Energy Metrics*

The normalized energy metrics for all images are listed in Table 4.1. The metrics for waveforms introduced in Chapter II are also included for comparison purposes. Using the normalized energy metrics listed, the percentage of aliased energy which has been removed from each image is computed by following the procedure listed in Section 2.6.2. Table 4.2 lists the percentage reduction from the LFM images and Table 4.3 lists the percentage reduction from the uncoded RSF images.

Tables 4.2 and 4.3 also list the ratio of the subpulse -3 dB bandwidths. The -3 dB bandwidths are measured from Figs. 2.7, 2.14, 3.1, 3.3 and 3.5. The bandwidth expansion of each subpulse is primarily responsible for the improved aliased energy mitigation. The overall waveform bandwidth, and hence the overall pulse compression ratio, is unchanged.

4.5   *Summary*

The research goal is to reduce the amount of Doppler aliasing present in WA-SAR images through the use of phase coded RSF waveforms. From Table 4.2 it can

Figure 4.7: (a) SAR image generated using RSF-P4 for $v_a = 100$ m/s with 60 dB dynamic range.
(b) Surface plot showing the relative amplitudes of the primary and aliased targets. The maximum values along ground range and cross range are projected onto the walls.
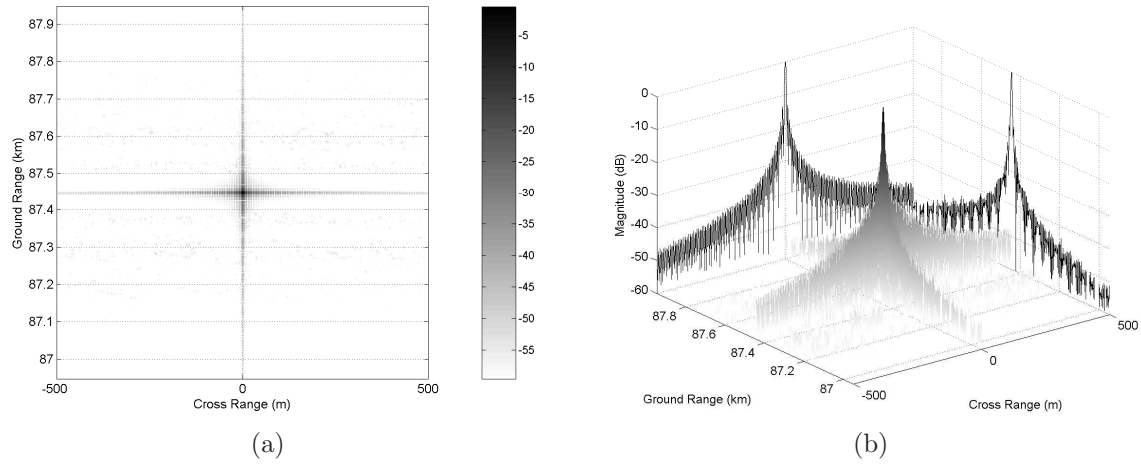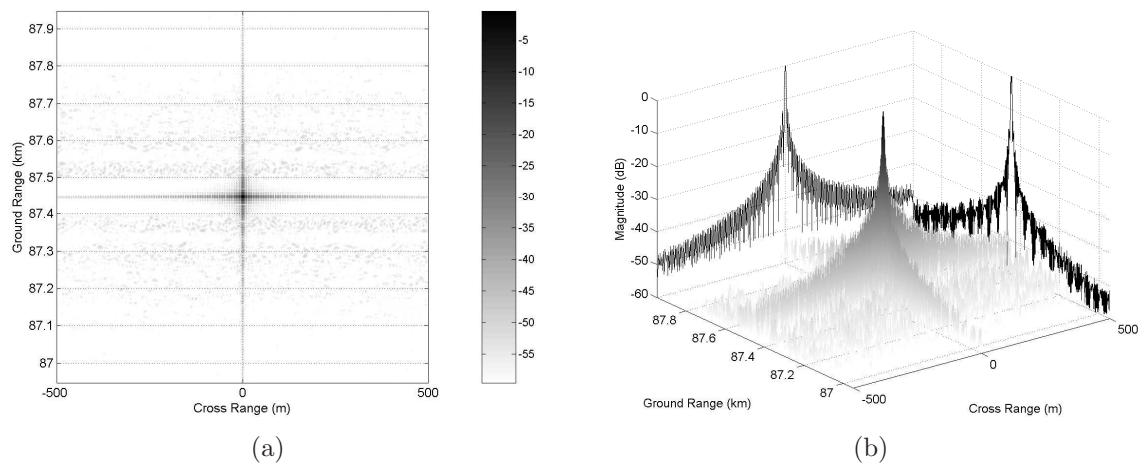

Figure 4.8: (a) SAR image generated using RSF-P4 for $v_a = 200$ m/s with 60 dB dynamic range.
(b) Surface plot showing the relative amplitudes of the primary and aliased targets. The maximum values along ground range and cross range are projected onto the walls.

Table 4.1:   Normalized Energy Metrics

Waveform	Normalized Energy Metric	
	$v_a = 100$ m/s	$v_a = 200$ m/s
LFM	3.45125	6.58012
RSF	1.10848	1.26160
RSF-LFM	1.10007	1.23701
RSF-Barker	1.00659	1.02107
RSF-Frank	1.00177	1.00877
RSF-P4	1.00204	1.00859

Table 4.2:   Percentage improvement from LFM. The ratio of subpulse bandwidths shows the increase in frequency coverage for a single subpulse. The overall waveform bandwidth, and hence the overall pulse compression ratio, is unchanged.

Waveform	% Aliased Energy Reduction from LFM		Subpulse 3 dB Bandwidth
	$v_a = 100$ m/s	$v_a = 200$ m/s	Ratio
RSF	95.57	95.31	1
RSF-LFM	95.92	95.75	1
RSF-Barker	99.73	99.62	3.11
RSF-Frank	99.93	99.84	15.36
RSF-P4	99.92	99.85	23.59

Table 4.3:   Percentage Improvement from uncoded RSF. The ratio of subpulse bandwidths shows the increase in frequency coverage for a single subpulse. The overall waveform bandwidth, and hence the overall pulse compression ratio, is unchanged.

Waveform	% Aliased Energy Reduction from Uncoded RSF		Subpulse 3 dB Bandwidth
	$v_a = 100$ m/s	$v_a = 200$ m/s	Ratio
RSF	-	-	1
RSF-LFM	7.75	9.40	1
RSF-Barker	93.93	91.95	3.11
RSF-Frank	98.37	96.65	15.36
RSF-P4	98.12	96.72	23.59

Table 4.4:   Aliased Energy Levels

Waveform	Aliased Energy Level (dB)		Improvement from uncoded RSF	
	$v_a = 100$ m/s	$v_a = 200$ m/s	$v_a = 100$ m/s	$v_a = 200$ m/s
RSF	-45.1	-41.3	0	0
RSF-LFM	-45.3	-41.6	0.2	0.3
RSF-Barker	-53.5	-50.7	8.4	9.4
RSF-Frank	-56.8	-53.9	11.7	12.6
RSF-P4	-56.2	-53.7	11.1	12.4

be seen that all waveforms eliminate at least 95% of the aliased energy present in the LFM waveform. The phase coded waveforms perform better than waveforms used in previous research (RSF, RSF-LFM) by removing at least 99% of the aliased energy which is present in the LFM images.

The percentage improvement of the phase coded waveforms with respect to the uncoded RSF waveform is impressive. At least 90% of the aliased energy remaining in the RSF image is removed by each of the phase coded waveforms. RSF-Frank and RSF-P4 waveforms perform better than RSF-Barker due to the fact that the code lengths are longer. Longer codes result in more spreading of the individual subpulse frequencies.

The uncorrupted dynamic range of the images also improves with phase coded waveforms. The relative amplitude of the aliased energy in each image is listed in Table 4.4. Remember, receiver noise is not modeled in this research. The background levels listed in Table 4.4 are entirely due to incomplete cancellation of aliased energy by the waveforms. The images can be floored just above the values listed in the table and the noise-like background will not appear. The RSF-Frank coded waveform allows the dynamic range of the image to be improved over RSF by 11.7 dB when the aircraft flies at 100 m/s and by 12.6 dB when the aircraft flies at 200 m/s. Such improvements allow finer detail to be visible in WA-SAR images.

V. Conclusions

This research investigates the benefit of using several phase modulated Random Stepped Frequency (RSF) waveforms in a Wide-Angle Synthetic Aperture Radar (WA-SAR) scenario. RSF waveforms have been demonstrated to have desirable auto-correlation properties which allow for cancelling of Doppler aliased scatterers in WA-SAR images [4]. Additional aliased energy reduction can be realized by improving the uniformity of the frequency coverage across the waveform's bandwidth [6]. This uniformity can be obtained by increasing the frequency coverage of each individual RSF subpulse. Phase modulation is a well known method for expanding the frequency content of signals and when applied to the RSF subpulses results in greatly improved aliased energy suppression and SAR image quality.

5.1   Results

Tables 4.2 and 4.3 show the percentage of aliased energy which has been eliminated from images formed in this research by using phase coded waveforms instead of LFM or uncoded RSF. The figures in these tables are for images with a 60 dB dynamic range. All RSF waveform variants reduce the aliased energy by at least 95.3%.

The phase coded RSF waveforms (RSF-Barker, RSF-Frank, and RSF-P4) which were introduced in this research effort all eliminate at least 99.6% of the aliased energy. RSF-Frank coded waveforms are the most effective for an aircraft velocity of 100 m/s with 99.93% energy reduction. At an aircraft velocity of 200 m/s (worst case aliasing) the RSF-P4 coded waveform is most effective with 99.85% energy reduction. Since images formed at the higher aircraft velocity have more aliased energy to mitigate, the RSF-P4 waveform's performance is notable.

The phase coded waveforms are also effective in significantly reducing the noise-like background which degraded previous images. Phase coded RSF waveforms lower the amplitude of aliased energy, allowing the uncorrupted noise-free dynamic range of the images to be improved substantially. The RSF-Frank coded waveform improves

61

the noise-free dynamic range by 12.7 dB under worst case aliasing (all possible targets aliased into the image).

The results of the research indicate that the noise-free dynamic range of WA-SAR images formed using RSF waveforms can be improved by almost 13 dB if the RSF-waveform subpulses are phase coded with a length 25 Frank code. The addition of dynamic range to WA-SAR images is especially important because small details will be more evident. While large targets may dominate the scene, often smaller, more subtle scatterers are of more interest to the SAR operator. Applications such as target recognition can utilize the additional detail to more accurately identify targets.

5.2 Future Work

This research utilized phase modulated RSF waveforms which expanded the bandwidth of each RSF subpulse. The overall effect of the individual subpulse bandwidth expansion is a bandwidth expansion of the entire waveform. Phase modulated waveforms no longer have nicely defined waveform bandwidths but significant frequency content extends beyond the bandwidth of the original RSF waveform. Hardware limitations such as limited amplifier bandwidths will cut-off the frequency spreading. According to [3] such bandwidth limitations will result in higher sidelobe levels and reduced gain from the matched filter. Implementation of a bandwidth limitation in the WA-SAR model would allow the impact of limited bandwidth processing in WA-SAR to be understood better.

Varying the code length of either the Frank or P4 may produce additional benefit. In this research both codes were of length 25. Further bandwidth expansion and corresponding image improvement is likely possible with longer codes. Such improvements are subject to the bandwidth limitations discussed previously.

Also, many other phase coded waveforms exist. Pseudonoise sequences, complementary codes (such as Golay or Welti codes) and Huffman codes are some examples. It is possible that other coding schemes will result in improved WA-SAR image quality.

62

A hardware implementation of WA-SAR would eliminate many of the remaining assumptions that remain in the computer models developed thus far. Real world data collects could be used to validate the simulated results achieved so far.

Bibliography

1. Bracewell, Ronald N. *The Fourier Transform and Its Applications (3rd ed.).* McGraw-Hill Higher Education, New York, USA, 2000. ISBN 0-07-303938-1.

2. Jakowatz, Charles V., Daniel E. Wahl, Paul H. Eichel, Dennis C. Ghiglia, and Paul A. Thompson. *Spotlight-mode Synthetic Aperture Radar: A Signal Processing Approach.* Springer Science+Business Media, Inc., New York, USA, 1996. ISBN 0-7923-9677-4.

3. Lewis, Bernard L., Frank F. Kretschmer, Jr., and Wesley W. Shelton. *Aspects of Radar Signal Processing.* Artech House, Inc., Norwood, MA, USA, 1986. ISBN 0-89006-191-1.

4. Luminati, Jonathan E. *Wide-Angle Multistatic Synthetic Aperture Radar: Focused Image Formation and Aliasing Artifact Mitigation.* Ph.D. thesis, Air Force Institute of Technology, Wright-Patterson Air Force Base, Ohio, USA, 2005.

5. Mahafza, Bassem R. *Radar Systems Analysis and Design Using Matlab.* Chapman & Hall / CRC, New York, USA, 2000. ISBN 1-58488-182-8.

6. McMahon, Jason. *Doppler Aliasing Reduction In Wide-Angle Synthetic Aperture Radar Using A Linear Frequency Modulated Random Stepped-Frequency Waveform.* Master's thesis, Air Force Institute of Technology, Wright-Patterson Air Force Base, Ohio, USA, 2005.

7. Moses, R., M. Cetin, and L. Potter. "Wide Angle SAR Imaging". *SPIE Algorithms for Synthetic Aperture Radar Imagery XI.* Orlando, FL, USA, Apr. 12-16 2004.

8. Oppenheim, Alan V., Ronald W. Schafer, and John R. Buck. *Discrete-time Signal Processing (2nd ed.).* Prentice-Hall, Inc., Upper Saddle River, NJ, USA, 1999. ISBN 0-13-754920-2.

9. Skolnik, Merrill I. *Introduction to Radar Systems (3rd ed.).* McGraw-Hill, New York, USA, 2001. ISBN 0-07-288138-0.

REPORT DOCUMENTATION PAGE

1. REPORT DATE *(DD–MM–YYYY)*	2. REPORT TYPE	3. DATES COVERED *(From — To)*
23–03–2006	Master's Thesis	Sept 2004 — Mar 2006

4. TITLE AND SUBTITLE

Doppler Aliasing Reduction In Wide-Angle Synthetic Aperture Radar Using Phase Modulated Random Stepped-Frequency Waveforms

5a. CONTRACT NUMBER

5b. GRANT NUMBER

5c. PROGRAM ELEMENT NUMBER

6. AUTHOR(S)

Andrew W. Hyatt, Capt, USAF

5d. PROJECT NUMBER

5e. TASK NUMBER

5f. WORK UNIT NUMBER

7. PERFORMING ORGANIZATION NAME(S) AND ADDRESS(ES)

Air Force Institute of Technology
Graduate School of Engineering and Management (AFIT/EN)
2950 Hobson Way
WPAFB OH 45433-7765

8. PERFORMING ORGANIZATION REPORT NUMBER

AFIT/GE/ENG/06-23

9. SPONSORING / MONITORING AGENCY NAME(S) AND ADDRESS(ES)

AFRL/SNRT
Attn: William Baldygo
2241 Avionics Circle
Wright-Patterson AFB, OH 45433
DSN: 587-4049 email: william.baldygo@rl.af.mil

10. SPONSOR/MONITOR'S ACRONYM(S)

11. SPONSOR/MONITOR'S REPORT NUMBER(S)

12. DISTRIBUTION / AVAILABILITY STATEMENT

Approval for public release; distribution is unlimited.

13. SUPPLEMENTARY NOTES

14. ABSTRACT

This research investigates the benefits of using several phase modulated Random Stepped Frequency (RSF) waveforms in a Wide-Angle Synthetic Aperture Radar (WA-SAR) scenario. RSF waveforms have been demonstrated to have desirable properties which allow for cancelling of Doppler aliased scatterers in WA-SAR images. Additional aliased energy reduction is realized by improving the uniformity of the frequency coverage across the waveform's bandwidth. Phase code modulations applied to the subpulses of a RSF waveform spread the subpulse frequency content and improve WA-SAR image quality. A length 13 Barker code applied to a RSF waveform produces an image with a 91.95% reduction in the aliased energy present relative to a WA-SAR image produced using uncoded RSF. Length 25 Frank and P4 coded RSF waveforms reduce aliased energy by 96.65% and 96.72% respectively. Additionally, phase coded RSF waveforms produce images with improved noise-free dynamic range capabilities. The Barker, Frank and P4 coded waveforms improve the noise-free dynamic range by 9.4 dB, 12.6 dB, and 12.4 dB, respectively.

15. SUBJECT TERMS

synthetic aperture radar, phase coding, wide-angle synthetic aperture radar, radar

16. SECURITY CLASSIFICATION OF:			17. LIMITATION OF ABSTRACT	18. NUMBER OF PAGES	19a. NAME OF RESPONSIBLE PERSON
a. REPORT	b. ABSTRACT	c. THIS PAGE			Maj. Todd B. Hale (ENG)
U	U	U	UU	78	19b. TELEPHONE NUMBER *(include area code)* (937) 255–3636, ext 4639